The water cycle

Aiguo Dai^a on and **Kevin E Trenberth**, aDepartment of Atmospheric and Environmental Sciences, University at Albany, SUNY, Albany, NY, United States; National Center for Atmospheric Research, Boulder, CO, United States; University of Auckland, Auckland, New Zealand

© 2025 Elsevier Inc. All rights are reserved, including those for text and data mining, Al training, and similar technologies.

Introduction	2
The water cycle	2
Physical processes of the water cycle	4
Evaporation and transpiration	4
Precipitation process	6
Runoff and infiltration	7
Expected response of the water cycle to global warming	8
Observed variations and changes in the water cycle	g
Atmospheric water vapor and clouds	9
Soil moisture, groundwater, mountain glaciers and polar ice sheets	10
Precipitation, evapotranspiration and continental discharge	13
Model-simulated response to global warming	15
Simulations of the water cycle in climate models	15
Model-simulated response of the water cycle	18
Summary and challenges	19
Acknowledgments	20
References	20

Abstract

The movement of water through the Earth system in the form of water vapor, liquid water and ice, and its impacts on Earth's climate are described along with the underlying physical processes and changes in response to human-induced heating. The main water reservoirs and key water exchanges are first discussed, followed by a detailed description of the underlying physical processes that determine the water exchanges. Some theoretical considerations and expected response of the water cycle to global warming are presented. Historical variations and changes in the water cycle are then discussed. Challenges in simulating the water cycle, including its storage components as water vapor and clouds and its exchanges with the surface involving precipitation and evapotranspiration are addressed. Finally, model-projected future changes in the water cycle are briefly discussed.

Keywords

Atmosphere; Climate change; Climate variability; Clouds; Evaporation; Glaciers; Global warming; Hydrological cycle; Oceans; Precipitation; Runoff; Transpiration; Water cycle; Water vapor

Key points

- Water is essential for life, shapes Earth's landscape as an agent of erosion, plays a crucial role for human society and Earth's weather and climate
- Driven by the energy cycle, gravity, and movement of the air and ocean currents, water constantly moves through the atmosphere, ocean, and land in various phases, forming the global water cycle
- Evapotranspiration allows surface water to enter the atmosphere, where it is transported away from the source and forms clouds and precipitation, which returns the water back to the surface
- Differences in oceanic evaporation and precipitation alter upper ocean salinity and density, which creates density gradients that drive ocean currents to restore the freshwater balance in the upper ocean
- While there is a good understanding of the underlying physical processes, such as formation of clouds and precipitation, evaporation and transpiration, the complexity is enormous and their representation in numerical weather and climate models remains a major challenge
- Greenhouse gas-driven changes in the water cycle, such as melting of glaciers, increases in extreme precipitation and intense tropical cyclones, decreases in rainy days and higher atmospheric evaporative demand, lead to major impacts, including sea-level rise, increased inland and coastal flooding, and more droughts and wildfires
- Variability in precipitation and other water fluxes in observations and model simulations is large, which complicates the detection of externally forced changes in the water cycle.

Introduction

Earth is a blue planet, with water covering around 71% of Earth's surface. Water is essential for the beginning and existence of life on Earth and likely on other planets too. Every living cell of all living things needs water to survive. Plants need liquid water during photosynthesis. All animals need to drink water to keep hydrated for normal body function, including evaporative cooling from perspiration. A person typically needs to drink 2–3 l of water each day. Access to potable freshwater is considered as a basic human right by the United Nations.

Acting as an agent of erosion, water also shapes the landscape on Earth over time. Rainwater, stream and river water, and freezing and thawing of water can break up rocks, help form soils and shape landscapes. From the Grand Canyon in the southwestern United States to the meandering river channels in the Amazon, many land surface features are created by the mighty power of moving water and ice over time.

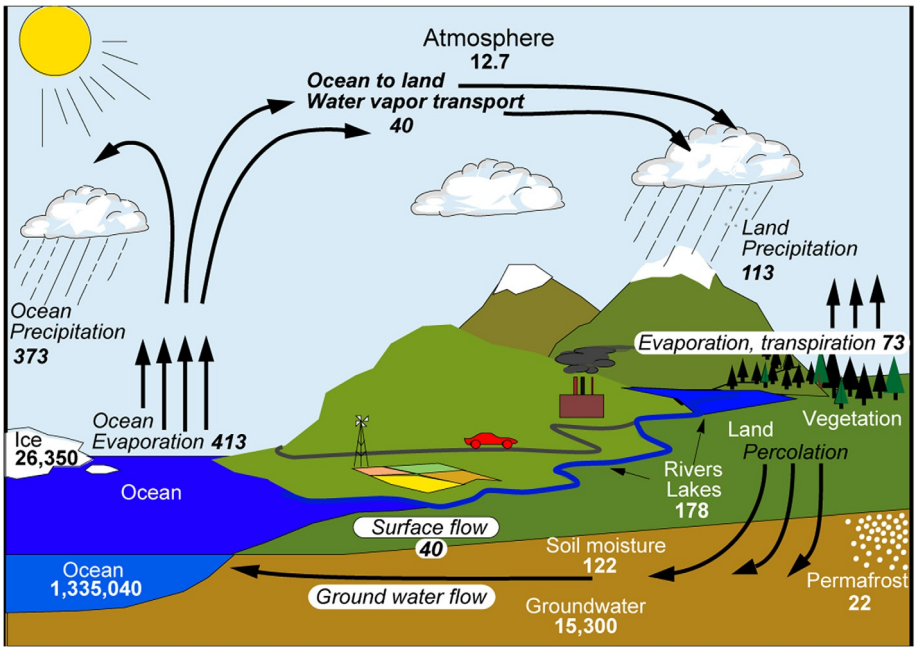
Water has also played a major role in human civilizations. A lot of water is needed to grow crops; it takes about 3000 l of water to produce food for one person's daily dietary need. Transportation over water (rivers and oceans) remains a key means of moving goods in global trade today. The energy harvested from falling or running water – hydroelectric power – continues to be a major source of energy for human society. The demise of some ancient civilizations, such as the Mayan civilization, may have been caused by changes in rainfall patterns, because rains were essential for growing enough crops to support a society.

Water plays a key role in Earth's weather and climate. Without water, a dry atmosphere would contain no clouds, no rainfall or snowfall, and no tropical cyclones. Without the greenhouse effect of water vapor in the atmosphere, the Earth's surface would be below the freezing point most of the time over most places. Water cycles through the Earth system – the atmosphere, ocean, and land – and largely regulates our weather and climate. It provides the available renewable freshwater resource over a land region. How the water cycle responds to human-induced global warming will largely determine the greatest impacts from ongoing climate change.

In this chapter, we describe the global water cycle – how water moves through the Earth system through various physical processes such as evapotranspiration and precipitation, and how these water cycle processes may have changed in recent decades and would change in the coming decades under ongoing climate change. It provides a comprehensive depiction of the global water cycle and a summary of the current knowledge on its changes.

The water cycle

The water cycle refers to the movement of water in the Earth system – the atmosphere, ocean, and land in the form of water vapor, liquid water and ice (Fig. 1). Although the estimates differ slightly among different sources, the oceans store most (close to 97%) of



Units: Thousand cubic km for storage, and thousand cubic km/yr for exchanges

Fig. 1 The reservoirs (plain font, in 10³ km³) and exchanges (in *slant font*, in 10³ km³/yr, equivalent to 10¹⁸ g yr⁻¹) of the global water cycle. Reproduced from Trenberth KE, Smith L, Qian T, Dai A., and Fasullo J (2007a) Estimates of the global water budget and its annual cycle using observational and model data. *Journal of Hydrometeorology* 8: 758–769 with permission. © American Meteorological Society.

the water on Earth as salty seawater. Only about 2.5% of Earth's water is freshwater, of which $\sim\!68\%$ is locked up in Antarctic and Greenland ice sheets and mountain glaciers and $\sim\!30\%$ is stored as groundwater below the land surface. Only about 1% of the freshwater is in surface water seen in lakes and rivers that provide most of the water used by humans.

When heated by solar radiation, water molecules at the ocean and land water surfaces may gain enough kinetic energy to break up the hydrogen bonds connecting individual water molecules to escape into the air, forming a water flux (referred to as evaporation) from the surface into the air. Water can also be evaporated from cavities inside leaves through a process called transpiration. Once in the air, water in the form of water vapor is moved around by winds, both horizontally and vertically. The capacity of the air to hold moisture is entirely dependent on air temperature following the Clausius-Clapeyron equation. Warmer air can hold more moisture and cooling air can increase the humidity to saturation, forming fog, cloud or even precipitation. Near the surface and in the lower troposphere (the lowest 12-18 km), the water holding capacity of the air increases exponentially with air temperature by about 7% per 1 °C warming.

Accordingly, when air cools, for example due to expansion during a rising motion or due to radiative cooling, vapor saturation levels, measured by RH, increase. As RH approaches 100%, water vapor starts to condense onto tiny particles (cloud condensation nuclei as a form of aerosols) to form cloud droplets, which may collide with each other to form bigger rain droplets that fall out of the cloud to produce precipitation. Precipitation is a general term and encompasses rainfall, snowfall and the deposition of many varied forms of ice such as hail, graupel (ice crystals), and sleet (a mix of rain and snow). Precipitation returns the evaporated water back to Earth's surface, although typically at a different location (often >1000 km away) from the original source, thus completing the water cycling from the ocean and land surfaces to the atmosphere and back (Fig. 1).

Over land, rainwater infiltrates and percolates into soil until it becomes saturated when it runs off down the terrain (Dingman, 2015). Horizontal runoff converges into streams and rivers, and the streamflow may take a few to several weeks to reach a river mouth on a coast and discharge into a sea. In a cold climate, snowfall may accumulate as snowpack on land, which melts during the late spring and early summer to generate peak streamflow, often in May–June for northern hemispheric rivers (Dai and Trenberth, 2002). Terrestrial evapotranspiration returns about 65% of land precipitation back to the atmosphere, with the remaining 35% running off the continents into the ocean mainly at the major river mouths (Dai and Trenberth, 2002), returning the \sim 10% of the oceanic evaporation that is transported by winds over land to form precipitation there.

A somewhat separate water cycle occurs in the ocean. This arises because the surface evaporation (E) exceeds precipitation (P) over the subtropical oceans, which makes seawater more saline and hence denser than other places. The upper ocean salinity and density gradients created by the P-E patterns (Fig. 2; Trenberth et al., 2011; plus the continental runoff, Dai and Trenberth, 2002) help drive the upper ocean currents, which attempt to remove the freshwater gradients created by the P-E imbalance by converging freshwater into the subtropical ocean, forming the water cycle in the oceans. Although the Hadley circulation plays a dominant role in the P-E distribution, other wind patterns also have some influences (Trenberth, 2022).

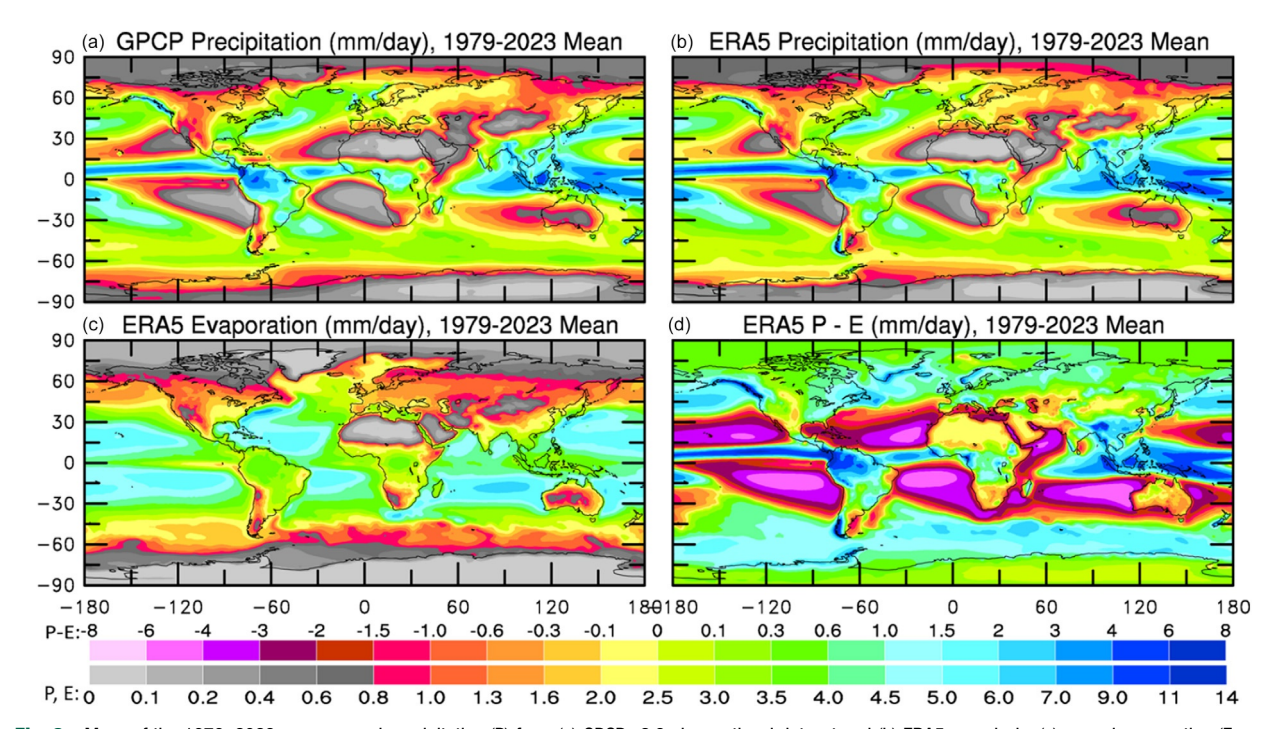


Fig. 2 Maps of the 1979–2023 mean annual precipitation (P) from (a) GPCP v2.3 observational dataset and (b) ERA5 reanalysis, (c) annual evaporation (E, including transpiration over land) from ERA5, and (d) ERA5 P-E difference. All are in units of mm/day. Map lines delineate study areas and do not necessarily depict accepted national boundaries.

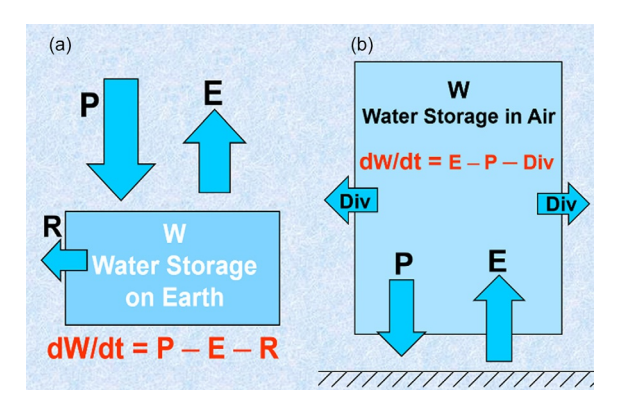


Fig. 3 Water balance analysis for (a) a land layer and (b) an atmospheric column. P = precipitation, E = evapotranspiration, R = runoff, Div = atmospheric divergence of water vapor, W = water storage in soil layer or the air column. Water is conserved during the regional and global water cycle.

On average, water molecules stay in the air for only about 10 days before being returned to the surface through precipitation as rain, hail, snow, freezing rain, or sleet. During this period, the water molecules have often been carried by wind more than 1000 km away from their original evaporation source. The residence time in the ocean is much longer (\sim 10³ years for interior ocean) and ranges from weeks (in rivers and plants) to years (in deep soils) over land. The main water exchanges (often referred to as "fluxes") include precipitation, evaporation over wet surfaces or transpiration by plants, runoff (R) and infiltration (i.e., the vertical water movement in the soil layer).

Most of the research on the water cycle is devoted to quantifying and understanding these water fluxes and their variations and changes over time (diurnal and seasonal cycles, annual-to-decadal variations and long-term trends). Changes in atmospheric water storage are relatively small compared to the accumulative amount (\approx 38 × the storage) of water by annual precipitation or evaporation (Trenberth et al., 2007a). Hence most water that goes into the air through evapotranspiration (ET or simply E) must come down through precipitation on annual and longer time scales; thus, for annual and long-term mean, global-mean P nearly equals E. This relationship also applies to future changes for global-mean P and E; that is, future global P change is closely linked to future global E change. On the other hand, changes in water storage, such as atmospheric water vapor content, are not directly linked to changes in the water flux such as precipitation, as different mechanisms control the water storages and water fluxes of the water cycle.

During the water cycle, water may change phase from liquid to gas (as during evaporation), or from gas to liquid or ice (as during precipitation); however, water is largely conserved on time scales shorter than a few hundred years as the loss to outer space and weathering of rocks, or exchanges through chemical reactions (e.g., methane oxidation) is very small compared with its total amount in the Earth system on such time scales. Thus, for a watershed (Fig. 3a) or an atmospheric column (Fig. 3b), the change in the water storage equals the difference between the incoming and outgoing water fluxes. For long-term mean, the storage change is relatively small compared to the annual water fluxes, so that runoff $R \approx P - E$ and atmospheric divergence of water vapor (Div) $\approx E - P$ (Fig. 3b). For the global atmosphere, Div = 0, so that global $P \approx \text{global E}$ for annual and long-term means.

Surface evaporation converts solar and other energy into latent energy stored in water vapor molecules, leading to a global latent heat flux of \sim 82 Wm⁻² from Earth's surface into the atmosphere (Trenberth, 2022). This energy is released to heat the atmosphere during formation of clouds and precipitation. Furthermore, clouds reflect about 78 W m⁻² of solar radiation to outer space, and help trap outgoing infrared or longwave radiation, together with water vapor and other greenhouse gases. Through these energy fluxes, the water cycle is closely coupled with the global energy cycle (Trenberth, 2022).

Physical processes of the water cycle

Evaporation and transpiration

On a water surface (e.g., of an ocean, lake, reservoir, or river) or a wet surface (e.g., of wet leaves or wet soils) exposed to unsaturated air, some water molecules may gain enough kinetic energy (e.g., from solar heating) to break the hydrogen bonds that connect the molecules together in a liquid or solid phase and enter the layer of air just above the water surface. The vapor molecules are then mixed upward away from the water surface, creating a water flux called **evaporation** (E). This evaporation process is the same over water and ice surface, soil pores, plant tissues, and cloud droplets. Thus, to sustain evaporation, a continued supply of water and energy is required along with mixing and removal of water molecules away from the water surfaces.

Inside tiny openings (stomata) on a leaf, liquid water needed to dissolve carbon dioxide for use in photosynthesis is also exposed to the air, and thus evaporation occurs inside the stomata as well (Fig. 4). This water flux, referred to as **transpiration**, is further regulated by the openings of the stomata. It becomes zero at night when stomata close and thus differs from the evaporation over a free water surface. The sum of evaporation and transpiration over a vegetated land surface is often called **evapotranspiration** (ET), with transpiration contributing 50–80% to the total ET over vegetated areas (Yang et al., 2023).

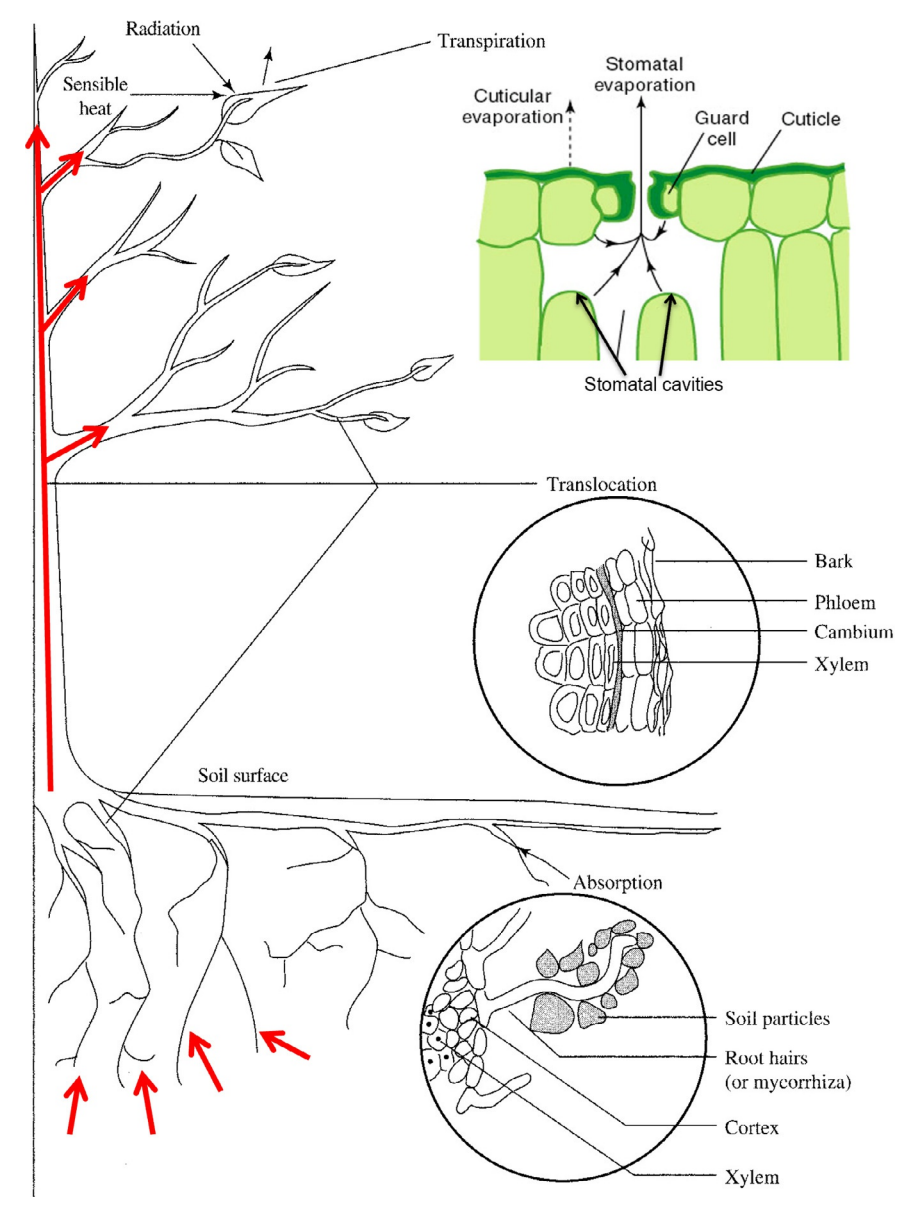


Fig. 4 The transpiration process: (1) absorption of soil water by plant roots; (2) translocation of water through the vascular system of the roots, stem, and branches to leaves; (3) movement of water through the vascular system of the leaf to the walls of tiny stomatal cavities, where evaporation occurs; and (4) the water vapor in these cavities moves into the ambient air through openings in the leaf surface called stomata, whose openings are controlled by the guard cell. Created by taking materials from Dingman SL (2015) *Physical Hydrology*, 3rd edn., Waveland Press, 643 pp and the website: https://courseware.e-education.psu.edu/simsphere/workbook/ch07.html.

Over a water surface, evaporation is controlled primarily by availability of energy (hence low E at night), wind speed which determines mixing, near-surface temperatures and RH which determine vapor pressure deficit (VPD). Over a vegetated land surface, ET is further controlled by vegetation and soil water. Typically, after a rainstorm, the land surface is wet and ET is high; as the surface soil dries up after a few days, ET then becomes dominated by transpiration of subsurface soil water (Dingman, 2015).

Most water molecules consist of one oxygen-16 atom (16 O), but a small faction contain a heavier oxygen-18 (18 O) atom. During evaporation, the lighter H_2^{16} O molecules will require less energy to escape the water surface and thus get evaporated preferably over the heavier H_2^{18} O molecules, thereby enriching the 18 O in the water reservoir. During the formation of clouds and precipitation, it is the opposite: the heavier H_2^{18} O molecules are condensed preferably over the lighter H_2^{16} O. This process – isotopic fractionation – during evaporation and precipitation creates fluctuations in the 18 O concentration in different water reservoirs, which allows scientists, especially paleoclimatologists, to track the water cycle.

Although E or ET can be measured directly using high-frequency sensers that can detect the high-frequency fluctuations in near-surface vertical wind and specific humidity, which can be used to derive the vertical water flux at a given site, continuous and

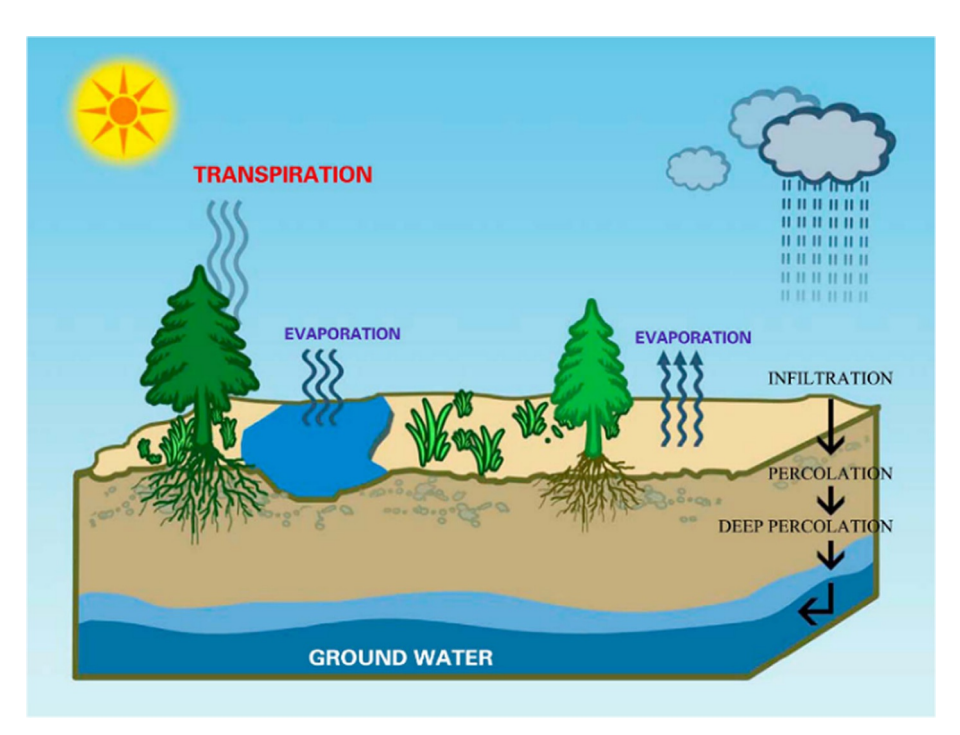


Fig. 5 Components of evapotranspiration include evaporation from a water body, wet leaves and soil surfaces, and transpiration from dry leaves, which extract soil water through their root systems. Reproduced from Wang K and Dickinson RE (2012) A review of global terrestrial evapotranspiration: Observation, modeling, climatology, and climatic variability. Reviews of Geophysics 50: RG2005, https://doi.org/10.1029/2011RG000373.

large-scale measurements of E over water and ET over land are impractical and unavailable over most of the Earth. Instead, E or ET is often estimated using various equations and near-surface meteorological data (Dingman, 2015). For E over a water surface, the bulk formula of the form: $E = C_q U (q_s - q_a)$ (where C_q is the turbulent exchange coefficient, U is near-surface wind speed, q_s is the surface saturation specific humidity and q_a is near-surface specific humidity) is often used for observational estimates and in numerical models. For ET over a land surface, the Penman-Monteith equation, which can be derived from the bulk formula and surface energy balance, is widely used (Dingman, 2015). Furthermore, in land surface models, ET is often estimated separately for its different components: evaporation from water, bare soil and vegetation surfaces, and transpiration by plants (Fig. 5; Wang and Dickinson, 2012). Uncertainties arise because the exchange coefficient can vary with wind speed and the nature of the surface.

The highest E occurs over the subtropical oceans, where clear skies allow most solar radiation to reach and heat the ocean surface and fairly steady trade winds occur, generating large evaporation (5–7 mm/day, Fig. 2c). Evaporation is low at high latitudes (<0.5 mm/day, Fig. 2c) due to low annual solar radiation and surface temperatures. Oceanic E is considerably higher than land ET for the same latitude, as ET is limited by available soil water over many drylands. Although E and ET have strong diurnal cycles following the solar heating that peaks around noon and is minimal during nighttime (Dai, 2024), it is less episodic or variable in both time and space than precipitation (Fig. 2). The spatial mismatch between E and P creates the P-E differences that drive the oceanic water cycle (Fig. 2).

Precipitation process

When air cools, for example due to expansion during an ascent or radiative cooling at night, water vapor can saturate and condense on tiny particles (cloud condensation nuclei or CCN), such as dust, ice, or salt, forming clouds. Small cloud droplets may collide with each other to form larger droplets (a process called coalescence), which may grow to rain droplets of 0.1-10 mm in diameter (d) that can fall out of the cloud base to produce precipitation. Hail forms in convective clouds when super-cooled (T < 0 °C) water droplets freeze to form hailstones, which can be blown into the upper part of the clouds by the storm's updraft (a rising air plume). As the updraft dissipates, the hailstones fall back to the lower part of the clouds. This process can repeat many times until the hailstones become large enough (d > 5 mm) to fall out of the cloud. Snowflakes form when tiny super-cooled cloud droplets freeze. Freezing rain occurs when snowflakes fall through a warm layer and melt, and re-freeze again before hitting the surface. Sleet (a mix of rain and snow or ice pellets (in the U.S.)) may form when the surface air temperature is just (1 °C-2 °C) above the freezing point (Dai, 2008).

Significant precipitation requires four ingredients: (1) cooling to saturation, often by upward motion in a storm, (2) condensation of water vapor to form clouds, (3) growth and fallout of cloud droplets, and (4) continued supply of water vapor into the precipitating storm. Upward motion can be generated by a warm front sliding upward over a cold airmass, atmospheric convection due to near-surface heating, or air flowing up hill (orographic lifting). Moreover, as condensation occurs, the phase change releases latent heat, which adds extra buoyancy and enhances upward motion.

The formation of cloud droplets requires the existence of tiny particles in the air, which are abundant in the polluted urban environment, leading to more numerous but smaller cloud droplets over urban areas. The growth of cloud droplets (of 10^{-2} mm in diameter) into rain droplets of 1 mm involves complex cloud microphysics, with collisions and coalescence between cloud droplets being the dominant process for warm clouds. In cold clouds with temperature around or below 0 °C, through the Bergeron-Wegner-Findeisen process ice particles can "steal" water from liquid particles as vapor evaporates from liquid droplets and condenses onto ice particles when the vapor pressure is between the saturation vapor pressure over ice (smaller) and water (larger). Cloud seeding, a human effort to modify weather, seeks to use this process to trigger or enhance precipitation by adding ice nuclei into a cloud. To produce significant precipitation, a storm needs to draw water vapor from the surrounding environment (often extending hundreds of kilometers away) through low-level convergence, which is partly driven by the buoyancy and updraft created by the latent heating within the storm.

Precipitation occurs only over a fraction (\sim 11%, Trenberth and Zhang, 2018) of Earth's surface at any given time and varies hugely in space. Indeed, precipitation is inherently intermittent (Trenberth et al., 2017). To fully characterize such a discontinuous variable it is essential to examine several characteristics, including (i) the accumulative amount (AA in mm depth, or divided by the accumulation time T to become the mean precipitation rate over T in mm/day: A = AA/T), (ii) the intensity (I, i.e., the precipitating rate averaged over the precipitating time t only, I = AA/t), and (iii) frequency (F, i.e., the fraction of time it precipitates, F = t/T). By definition, $A = F \times I$, which yields $\Delta A/A_o \approx \Delta F/F_o + \Delta I/I_o$ for small changes; that is, the percentage change in A (from A_o) is approximately the sum of the percentage changes in F and I. This simple relationship provides a very useful argument regarding future changes in F and I (Trenberth et al., 2003). For the same A, differences in F and I can result in very different land surface conditions and runoff (Fig. 6), although only A is often used to quantify precipitation at a given location. We argue that F and I, whose estimates require high-frequency data, should be used more often in quantifying precipitation in observations and models.

Annual mean precipitation rate (A) is determined mainly by the energy available for ET for the global mean (~2.7 mm/day) and it varies greatly from 6 to 10 mm/day in the Inter-Tropical Convergence Zone (ITCZ) to about 0.5 mm/day in the Arctic and less than 0.2 mm/day over deserts and Antarctica (Fig. 2). The polar regions are dry owing to cold air that can hold little moisture, while the heavy precipitation in the ITCZ and the lack of precipitation over the subtropical regions are due to the ascending and descending motions of the Hadley circulation, respectively. During a descent, air gets compressed (due to higher pressures at lower levels) and warms up, leading to lower RH which suppresses formation of clouds and precipitation. During an ascent within ITCZ, air expands and cools, leading to vapor saturation and formation of clouds and precipitation.

On the other hand, precipitation intensity (*I*) is controlled by primarily temperature through the Clausius-Clapeyron equation that determines the water vapor holding capacity of the air, and thus largely the amount of water vapor in the air. The latter determines the amount of moisture convergence and thus precipitation amount from a storm.

Aside from the subtropical oceans and arid land areas, annual precipitation usually exceeds evaporation or evapotranspiration (Fig. 2d), leading to some runoff over land. As precipitation occurs over a much smaller fraction of time than evaporation, the intensity of P is much higher than E. Evaporation cools the surface (evaporative cooling) while precipitation heats the atmosphere (latent heating). Whereas evaporation is controlled mainly by surface heating and wind speed, precipitation is determined by atmospheric circulation and water vapor content.

Runoff and infiltration

At the start of a rainstorm over land, rainwater infiltrates downward into the unsaturated soil layer, generating a downward water flux referred to as **infiltration** or **percolation**. As the soil becomes saturated or when the rain rate exceeds the infiltration rate, lateral water flow occurs, generating **runoff**. Runoff refers to the lateral flow of water either on land surface (surface runoff) or below the surface (subsurface runoff or return flow), often following the terrain under gravity and converging into streams and then rivers.

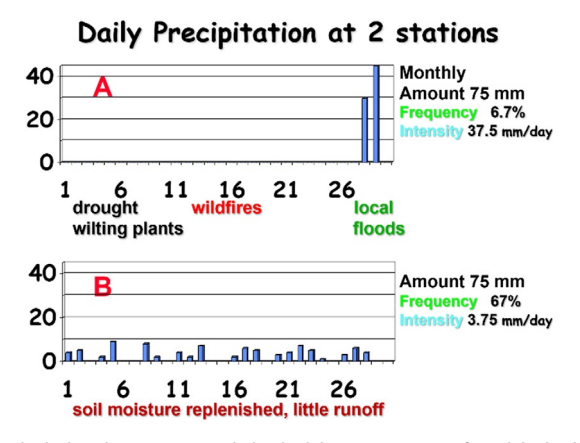


Fig. 6 Daily precipitation events at two hypothetical stations over a month that had the same amount of precipitation but very different precipitation frequency and intensity, as well as different impacts on land surface conditions and runoff. From Trenberth KE (2011) Changes in precipitation with climate change. *Climate Research* 47: 123–138. https://doi.org/10.3354/cr00953.

The ratio of runoff to precipitation (*C*, referred to as the runoff coefficient or runoff ratio) over a watershed is a crucial parameter in flood forecasting. It depends on the surface type (*C* ranges from over 0.7 in urban areas to 0.1–0.3 over vegetated surfaces to below 0.1 over deserts and drylands), terrain slope, saturation level of the ground, catchment size, and the rainfall intensity and duration (Dingman, 2015).

Annual runoff determines the available renewable freshwater resource at a given region. Over global land, runoff generates about $38,000 \text{ km}^3/\text{yr}$ freshwater discharge into the oceans, primarily at the mouths of world's major rivers (Dai and Trenberth, 2002). This discharge flux is about 10 times the annual total freshwater used by human society, including the water used in irrigation. However, because of the uneven distribution of the discharge (i.e., mainly in the tropics and mid-high latitudes, with the Amazon River accounting for \sim 17% of the total continental discharge, Dai and Trenberth, 2002), many drylands in the subtropics and other regions face severe water shortages.

In the absence of rainfall on land, the surface dries out and any vegetation begins to wilt. This process depends on the plant and root depths and ultimately dries out the subsurface. This can lead to soil cracking, as the soil shrinks. This process firstly makes the vegetation vulnerable for wildfire, and secondly, makes the infiltration of subsequent rains very uneven and can lead to erosion. In areas of slope, it may lead to failure of the terrain as chunks break off and perhaps mud slides during a subsequent rainstorm.

Expected response of the water cycle to global warming

Many aspects of the water cycle are expected to change in response to increasing greenhouse gases (GHGs) and aerosols simply based on some theoretical considerations (Trenberth et al., 2003; Trenberth, 2022; Trenberth and Cheng, 2024), which can help us understand model-projected changes discussed in Section "Model-simulated response to global warming." Theory predicts an acceleration of the global water cycle in response to global warming, with increasing global-mean evaporation *E* and precipitation *P*, as well as increasing precipitation intensity and more continental runoff. Because the amount of moisture in the atmosphere is quite small, any increase in global evaporation must be matched by the same increase in global precipitation on an annual basis (Fig. 3).

As climate warms, global precipitation amount is expected to increase as it is controlled by energy changes and surface evaporation. Climate models predict about 1%–3% increase in global *E* and *P* per 1 °C surface warming under future emissions scenarios, which include the effects of future emissions of aerosols (Collins et al., 2013). At the surface, increased heating from elevated GHGs and higher air temperatures should lead to more evaporation, although changes in vertical mixing rates, which depend on projected atmospheric stability and convection, could provide additional control on the *E* change. In the atmosphere, more GHGs accelerate increases in downward longwave (LW) radiation through higher emissivity, allowing it to increase faster than surface upward LW radiation as the temperature increases similarly at the surface and in the lower troposphere. This should result in a net LW cooling of the atmosphere, balanced by increased latent heating from precipitation, leading to more precipitation under GHG-induced global warming. However, changes in anthropogenic aerosols may act to short-circuit the water cycle (Trenberth, 2022). Carbonaceous aerosols with brown or black color heat the atmosphere directly by absorbing sunlight but reduce solar heating at the surface, taking latent heating and thus precipitation out of the water cycle loop (i.e., with reduced E and P). Sulfate aerosols form a whitish veil that reflects sunlight to the outer space, reducing surface heating and thus evaporation. Increases in these aerosols cause surface cooling and reduce evaporation and precipitation, thus partially offsetting the enhancement of the water cycle from increasing GHGs. Climate models still struggle in simulating aerosol impact on clouds and precipitation, which increases the uncertainties in model-projected global *P* response to given emissions of GHGs and aerosols.

Besides the precipitation amount increase, other precipitation characteristics are also expected to change under global warming (Trenberth et al., 2003). Precipitation intensity during a storm is determined by the amount of low-level moisture convergence, which is largely controlled by atmospheric moisture content. As air temperature rises, the moisture holding capacity in the lower troposphere increases by about 7% per 1 °C warming based on the Clausius-Clapeyron relation, which increases atmospheric demand for moisture. Over oceans and other wet surfaces where water supply is unlimited, atmospheric moisture should follow the demand increase and rise by about 7%/°C. This should lead to only small changes in atmospheric RH (Gulev et al., 2021), which means that atmospheric moisture should increase by about 7%/°C under global warming over oceans and non-arid regions. Thus, for the same air mass convergence into a storm, the moisture convergence and thus precipitation amount produced by the storm (i.e., precipitation intensity *I*) should increase by about 7%/°C under global warming. The extra latent heating could further enhance the upward motion and thus low-level convergence, leading to even larger increases in heavy precipitation during a storm (Trenberth, 2011). This could also alter storm duration and possibly lead to bigger storm sizes (Dai et al., 2020), and each factor can further increment the total precipitation from a storm to the order of 30%/°C (Trenberth, 2011; Trenberth et al., 2018).

As explained in Section "Precipitation process," the percentage change in precipitation amount A equals to the sum of the percentage changes in precipitation frequency F and intensity I: $\Delta A/A_o \approx \Delta F/F_o + \Delta I/I_o$. Given that $\Delta A/A_o = 1\%-3\%/^{\circ}C$ and $\Delta I/I_o \geq 7\%/^{\circ}C$, it requires the frequency to decrease (Trenberth et al., 2003). Note that $F = t/T = D \times N/T$, where t is the precipitating time, T is the observation time period, D is the mean duration of precipitation events, and N is the number of precipitation events. Thus, the frequency decrease can result from a decrease in D or N or both. As explained in Section "Model-simulated response of the water cycle," the precipitation frequency decrease results from a decrease in light-moderate precipitation events while heavy precipitation events increase. How the duration (D) for these different events would change is unclear. A decreasing precipitation frequency means longer dry spells between rainstorms, while stronger precipitation intensity will result in more heavy

precipitation, higher runoff and possibly more flooding. Both changes could lead to drier soil (Dai et al., 2018) and increased hydroclimate volatility (Swain et al., 2025).

Another expected change is the phase of precipitation, which changes rapidly from solid (snow) to liquid (rain) as surface air temperature increases from zero to 4 °C (Dai, 2008). This snow-to-rain phase change should occur around the freezing line mainly in spring and autumn in the midlatitudes. It should reduce snow accumulation on the ground, although mid-winter snowfall could increase as atmospheric moisture increases with air temperature. Surface warming should melt snowpack more quickly in spring, resulting in diminished streamflow in summer in the western U.S., the Andes, and other mountainous regions, where snowmelt water is a major freshwater resource during summer.

The faster increase in atmospheric water vapor than in global precipitation amount suggests that the mean residence time of water molecules in the atmosphere may increase slightly under global warming. However, this does not mean that the global water cycle is slowing down, as the main water cycling fluxes (global P, E and R) are expected to increase under global warming.

As atmospheric water vapor increases, more moisture is transported from ocean to land under global warming. More intense precipitation may also increase surface runoff. These changes should increase continental runoff (Fig. 1). Melting land-ice also contributes a little.

As discussed in Sections "Observed variations and changes in the water cycle" and "Model-simulated response to global warming," most of the expected changes discussed above are confirmed in observations and model projections with increasing GHGs.

Observed variations and changes in the water cycle

Variations and long-term changes in the reservoirs and fluxes of the water cycle (Fig. 1) are of great concern and thus are a major research topic in Earth science. However, it has been challenging to quantify and understand long-term changes in the water cycle owing to a lack of reliable long-term observations (Hegerl et al., 2015). Below we briefly discuss the observed historical changes and variations in atmospheric water vapor and clouds, soil moisture, groundwater, glaciers and icesheets (reservoirs), and precipitation, evapotranspiration and continental runoff (fluxes). More detailed reviews can be found in Trenberth et al. (2007b), Hartmann et al. (2013), and Gulev et al. (2021). It should be emphasized that any observed changes in precipitation and other water fluxes can result from both unforced natural variations (such as El Niño-Southern Oscillation ENSO) and externally forced changes, and natural variability often dominates the changes at local and regional scales especially for relatively short periods (e.g., \leq 60 years) (Deser et al., 2012; Dai and Bloecker, 2019).

Atmospheric water vapor and clouds

Atmospheric water vapor consists of a tiny fraction of the total water on Earth (Fig. 1), yet it plays a crucial role in Earth's weather and climate. Although water vapor is the most important GHG in today's climate, it is short lived (\sim 10 days) and depends critically on atmospheric temperatures that are determined by longer-lived GHGs. Consequently, water vapor provides strong positive feedback that roughly doubles the direct warming from a CO₂ increase (Schmidt et al., 2010), rather than a forcing with respect to climate change. Water vapor can be transported by winds from one place to another quickly and provides the water sources for forming clouds and precipitation.

Water vapor content near the surface is derived from measurements by psychrometers (consist of a dry-bulb and a wet-bulb thermometer) before the automation of weather stations (started in the late 1990s) and by capacitive sensors since the automation, which may cause some discontinuities in surface humidity and water vapor records (Ingleby et al., 2013). In the atmosphere, water vapor is measured by humidity sensors in radiosondes around the world since the late 1950s (mainly over land and islands) and by satellite remote sensing since 1987. The radiosonde humidity records contain large artificial changes resulting from humidity sensor changes over time that need to be removed through homogenization; however, they have often been used by atmospheric reanalyses and other applications without homogenization, thereby giving misleading results (Dai et al., 2011; Wan et al., 2024).

Observations indicate that near-surface and upper-air water vapor content has been rising in tandem with air temperature (Figs. 7–8; Wang et al., 2016), despite a decline in near-surface RH over land (Fig. 7; Dunn et al., 2024). The causes of the recent RH decline may include (1) spurious decline due to instrumental changes (Li et al., 2020), (2) a drier and hotter land (Dai, 2021), and (3) slower warming over oceans (Wan et al., 2024) which provide about 1/3 of the moisture for land precipitation (Fig. 1); hence even as the specific humidity increases over land, land RH may drop due to its faster warming (Fasullo, 2011). Atmospheric water vapor has been increasing roughly following the ~7%/K rate of saturation vapor pressure in areas where there is ample surface water. Large interannual PW variations are associated with ENSO throughout the Pacific.

Cloud cover was traditionally observed by a trained human, but automation of weather stations since the late 1990s has interrupted the cloud record (Dai, 2006; Warren et al., 2007), while satellite observations of clouds often contain inhomogeneities from changing satellite orbits and instrumentation and changing orbits (Norris and Evan, 2015; Stubenrauch et al., 2024). Station reports indicate that cloud cover increased from the 1950s to the early 1980s over many land areas, leading to decreased diurnal temperature range (DTR) over land (Dai et al., 1997, 1999); since then, it has decreased slightly, leading to increased DTR in recent decades (Dai, 2006; Zhong et al., 2023). From 1972 to 1996, cloud cover showed a large decrease over South America, small decreases for Eurasia and Africa, and no trend for North America (Warren et al., 2007). Annual cloud cover and precipitation

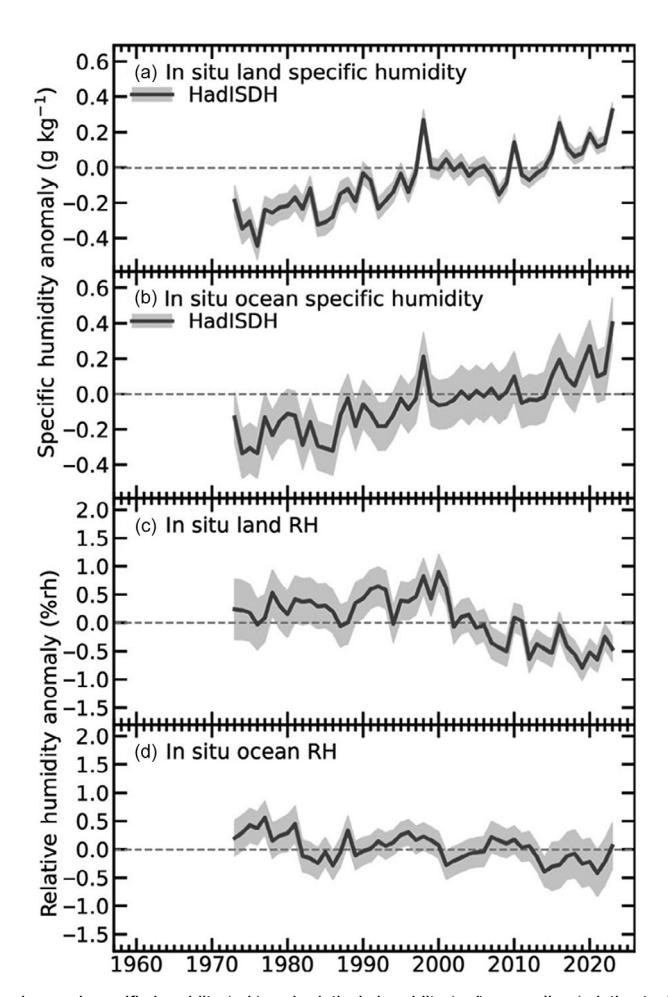


Fig. 7 Time series of surface observed annual specific humidity (a-b) and relatively humidity (c-d) anomalies (relative to 1991–2020 mean) from 1973 to 2023 averaged over global land (a, c) and ocean (b, d). Reproduced from Dunn RJH, Blannin J, Gobron N, Miller JB, and Willett KM (eds.) (2024) Global climate [in "state of the climate in 2023"]. Bulletin of the American Meteorological Society (BAMS), vol. 105: S12–S155. https://doi.org/10.1175/BAMS-D-24-0116.1 with permission. © American Meteorological Society.

anomalies are correlated (Dai et al., 1997), which increases confidence in these records. Changes in cloud cover are coupled with changes in surface solar radiation and land surface conditions (e.g., soil moisture; Zhong et al., 2023). They are partly related to decadal changes in anthropogenic aerosols as well as decadal variations in sea surface temperatures (SSTs) and climate.

Over the oceans, notably since 2000, there is a poleward movement of mid-latitude storm tracks and jet streams, expansion of subtropical dry zones, a narrowing of the tropical intertropical convergence zone (ITCZ), and increasing height of the highest cloud tops at all latitudes (Norris et al., 2016; Tselioudis et al., 2024; Trenberth et al., 2025), consistent with model-simulated responses to recent external forcing (Norris et al., 2016).

Soil moisture, groundwater, mountain glaciers and polar ice sheets

Historical records of soil moisture from in-situ measurements are sparse. Because of limited in-situ measurements, soil moisture over global land is often estimated by land surface models and through satellite remote sensing with varying performance (Beck et al., 2021). The model-derived soil moisture products often perform better when forced with high-resolution observed precipitation. Fig. 9 shows changes in soil moisture from ERA5-Land, a land surface model simulation forced by ERA5 meteorological data on 0.1° grids (Muñoz-Sabater et al., 2021), which has average performance in a comprehensive evaluation (Beck et al., 2021). ERA5-Land shows that soil moisture increased from 1950 to 1978 over central and southern Africa, southern and central Europe, northeastern South America, most North America and many parts of Asia. It decreased from 1979 to 2024 over most land areas (Fig. 9), consistent with the drying trend seen in drought indices that partly resulted from increased VPD under rising air temperatures (Dai, 2021). The recent regional soil drying trends over China and central Aisa are linked to decreasing precipitation and rising temperatures (Cheng et al., 2015; Zhu et al., 2022).

Groundwater levels have been declining during recent decades over many drylands with extensive croplands, such as the western U.S., the Middle East, southern and northern India, northern China, due to excessive withdrawals for irrigation (Jasechko et al., 2024; Kuang et al., 2024). Satellite observations show declining total water storage during 2002–2022 over southwestern and

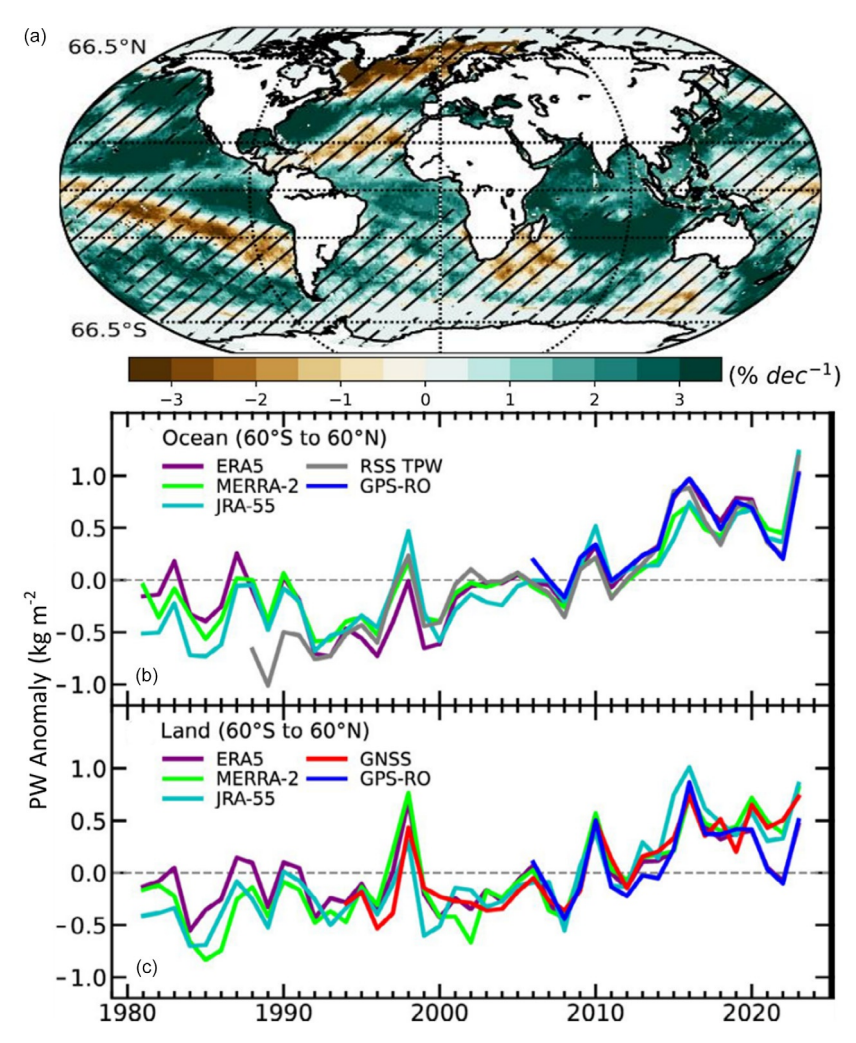


Fig. 8 (a) Linear trend map for annual total precipitable water (PW) during 2003–2021 estimated based on satellite microwave measurements. The stippling indicates the trend is insignificant at the 5% level. (b-c) Anomaly time series of annual PW averaged over global (60°S–60°N) (b) ocean and (c) land areas derived from three reanalyses (ERA5, MERRA-2 and JRA-55) and satellite microwave (RSS TPW) and GPS (GPS-RO and GNSS) observations. Map lines delineate study areas and do not necessarily depict accepted national boundaries. (a) Reproduced from Wan N, Lin X, Pielke RA Sr, Zeng X, and Nelson AM (2024) Global total precipitable water variations and trends over the period 1958–2021. *Hydrology and Earth System Sciences* 28: 2123–2137, https://doi.org/10.5194/hess-28-2123-2024. (b, c) Reproduced from Dunn RJH, Blannin J, Gobron N, Miller JB, and Willett KM (eds.) (2024) Global climate [in "state of the climate in 2023"]. *Bulletin of the American Meteorological Society (BAMS)*, vol. 105: S12–S155. https://doi.org/10.1175/BAMS-D-24-0116.1 with permission. © American Meteorological Society.

northwestern North America, southeastern Brazil, southern Europe, the Middle East, northern India, and North China, but increasing storages over eastern North America, central Africa, and southeastern China (Fig. 10; Scanlon et al., 2023).

Mountain glaciers were close to steady states during the 1960s but started to lose ice in the late 1970s (Fig. 11) when global temperature began to rise (Hugonnet et al., 2021; WGMS, 2023). Since 1950, global reference glaciers have cumulatively lost an ice mass of more than 30 m.w.e. per square meter of ice cover (Fig. 11; WGMS, 2023), which corresponds to a mass loss of >30,000 kg per square meter of ice cover or a glacier-wide ice thickness loss of >33 m.

The best ice-related record is probably that of sea ice extent in the Arctic, which has decreased by about 45% since 1979 in September, when the annual minimum occurs (Trenberth, 2022). The ice extent is readily determined from satellite observations because microwave measurements can see through cloud, although they are confounded by surface melt ponds of water.

Ice sheet melt or gain is fairly well measured by satellite laser altimetry since 2003. Ice sheets gain mass through snow accumulation and lose it through (i) surface melt runoff (Greenland, 50%–65%); (ii) iceberg calving (Antarctica, ~50%, and Greenland, 15%–25%); and (iii) basal melting of floating ice shelves (Antarctica, ~50%) and tidewater glaciers (Greenland, 15%–25%) (Trenberth, 2022). Greenland has a sea level rise potential of about 7 m if it all melted, and there has been widespread thinning of the ablation zone and thinning and retreat of tidewater glaciers. Antarctic ice has a sea level rise potential of about 58 m. Ice sheet gains have occurred in East Antarctica from increase snowfall accumulation while in West Antarctica basal melting of ice shelves is occurring owing to warmer waters in the surrounding ocean, reducing their buttressing capability and increasing ice discharge into the ocean.

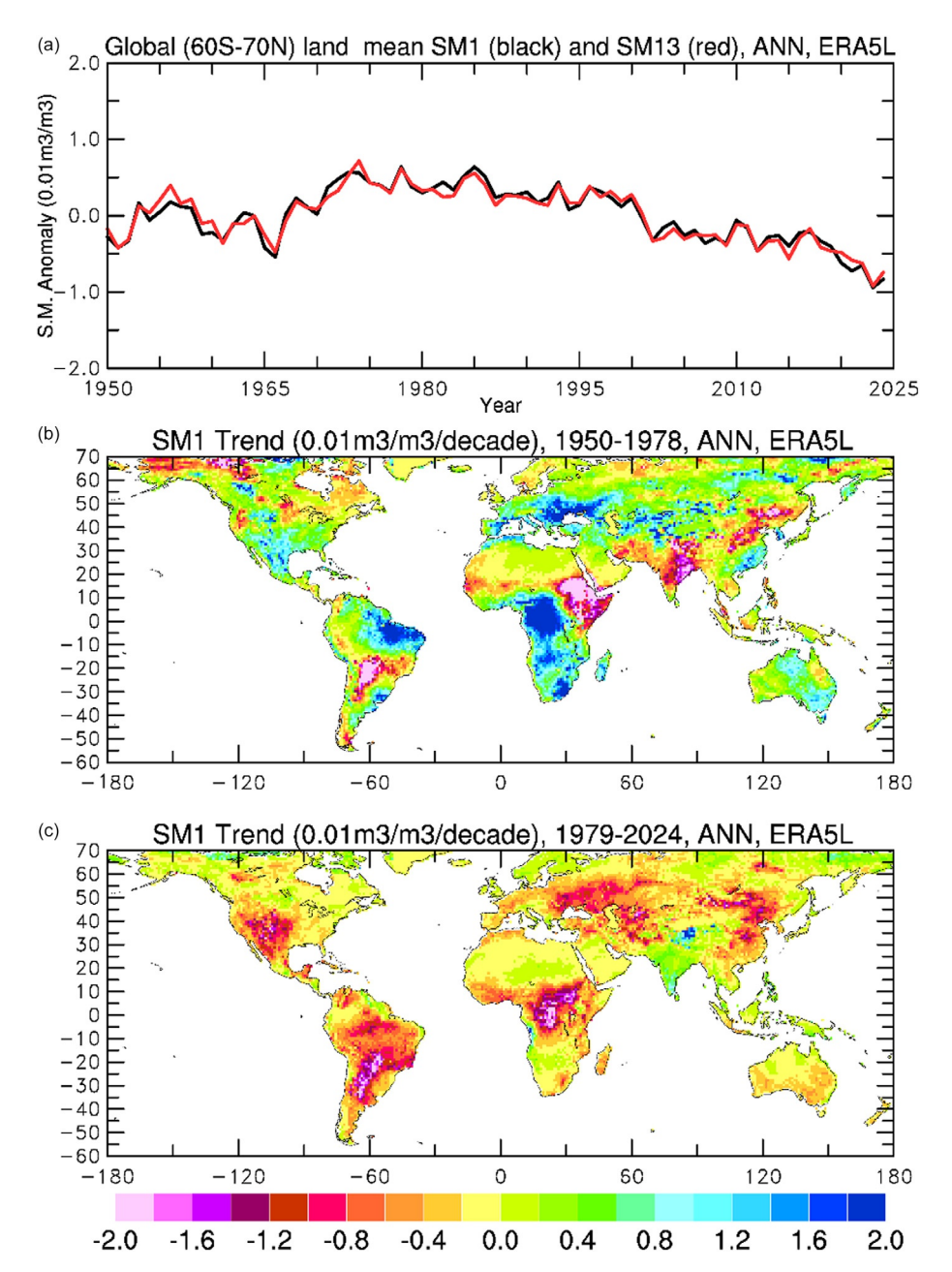


Fig. 9 (a) Anomaly time series of annual soil moisture averaged over land areas within 60° S-70° N within the top 7 cm (black) and top 1 m (red) layers, and (b-c) linear trend maps of annual soil moisture of the top 7 cm layer (similar for the top 1 m layer) during (b) 1950–1978 and (c) 1979–2024 based on ERA5-Land data. Map lines delineate study areas and do not necessarily depict accepted national boundaries.

Recent assessments (Smith et al., 2020; Trenberth, 2022) put the overall ice sheet mass change for Greenland between 2003 and 2019 at -200 ± 12 Gt/year, with accumulation in the high interior, and melt around the coast. The sea level equivalent change for this period is 8.9 mm. This value is somewhat less than another recent estimate (-268 ± 14 Gt/y) (Mouginot et al., 2019). What is clear is that melting of Greenland has accelerated since 2006.

In Antarctica, the ice sheet has gained mass from snowfall, especially over East Antarctica, but has lost mass through melting ice shelves and calving. There has been thickening along the steep slopes of the Antarctic Peninsula and around the coast, while East Antarctica gained some mass from snow accumulation. However, these gains were more than offset by ongoing mass loss around the margins, especially West Antarctica, since 2003 in response to rapidly shrinking ice shelves. Hence from 2003 to 2019, according to Smith et al. (2020), while East Antarctica is estimated to have gained 196 Gt/y (106 floating, 90 grounded), West Antarctica lost about 245 Gt/y (-76, -169), and the Antarctic Peninsula lost a further 53 Gt/y (-14, -39), for a net loss of Antarctic ice of about 103 Gt/y (15, -118), but with quite a large uncertainty from the floating ice component (15 ± 65 Gt/y) (Trenberth, 2022).

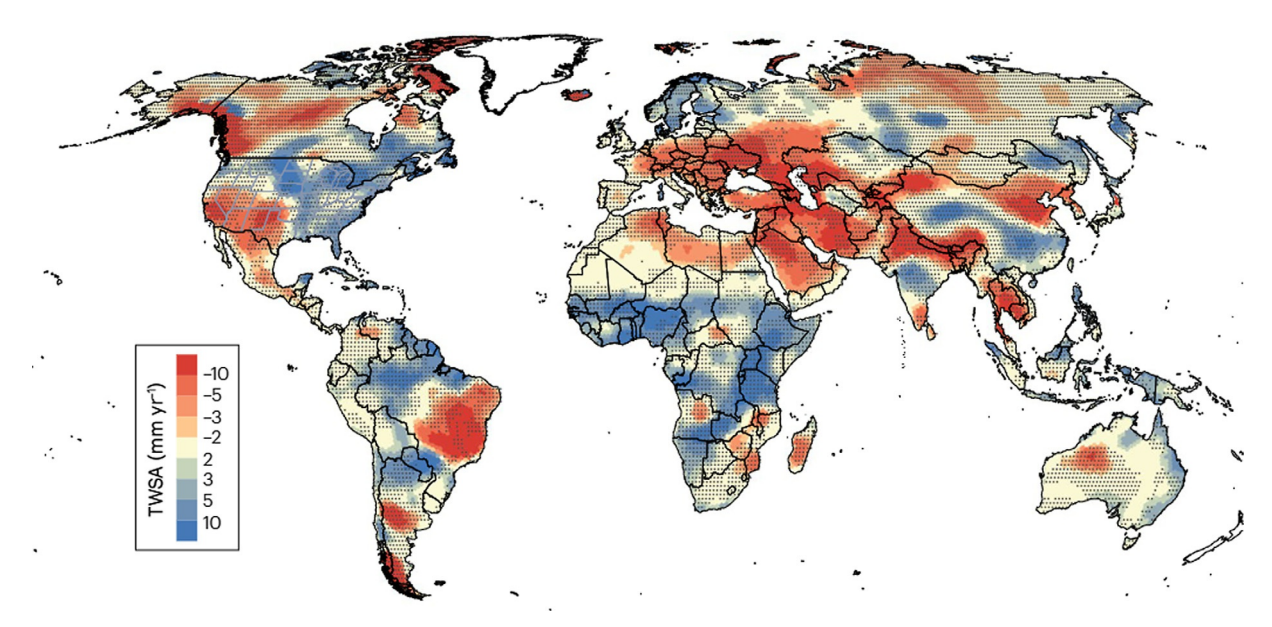


Fig. 10 Linear trends (in mm/yr) during 2002–2022 in total water storage (TWS) estimated from GRACE satellite data. Stippling indicates the change exceeds three standard deviations of interannual variability. Map lines delineate study areas and do not necessarily depict accepted national boundaries. Reproduced from Scanlon BR et al. (2023) Global water resources and the role of groundwater in a resilient water future. Nature Reviews Earth and Environment 4: 87–101 with permission.

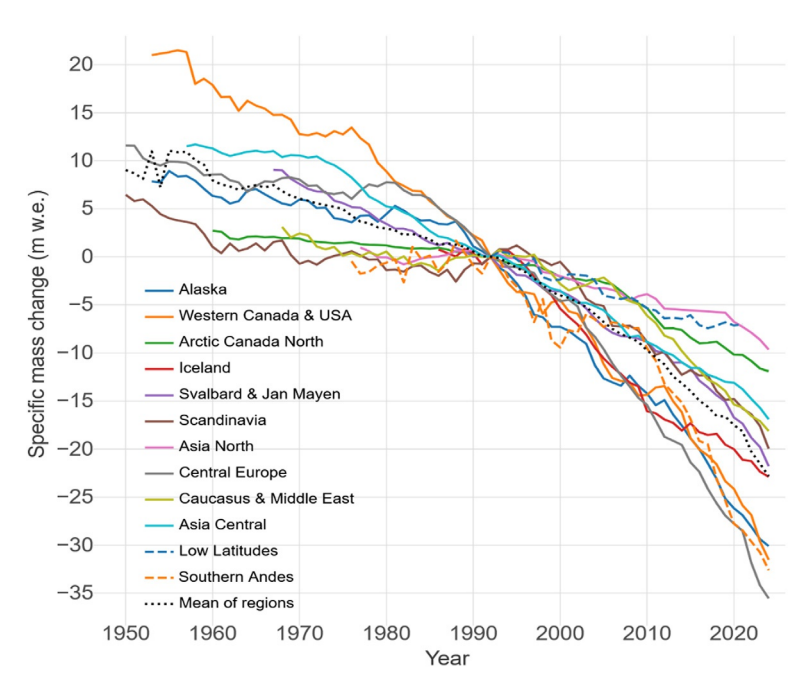


Fig. 11 Cumulative mass change relative to 1992 (in units of meter water equivalent) for regional and global means based on data from reference glaciers. Reproduced from https://wgms.ch/global-glacier-state/.

Precipitation, evapotranspiration and continental discharge

Many studies have examined historical precipitation changes over various land areas based on rain-gauge records; however, over oceans precipitation estimates are available only since 1979 when satellite observations began. Rain-gauge data suggest that precipitation over land increased slightly by 1.4%–2.3%/century from 1901 to 2023, primarily over the northern mid-high latitudes, southeastern South America, and most of Australia (Fig. 12). Over shorter periods and at the local and regional levels, precipitation trends are often dominated by noisy natural variability, such as decadal-multidecadal variations in Pacific and Atlantic SSTs (Dong and Dai, 2015; Qin et al., 2022) (Fig. 13). During 1979–2023, the trend in global-mean precipitation is insignificant (Fig. 13a),

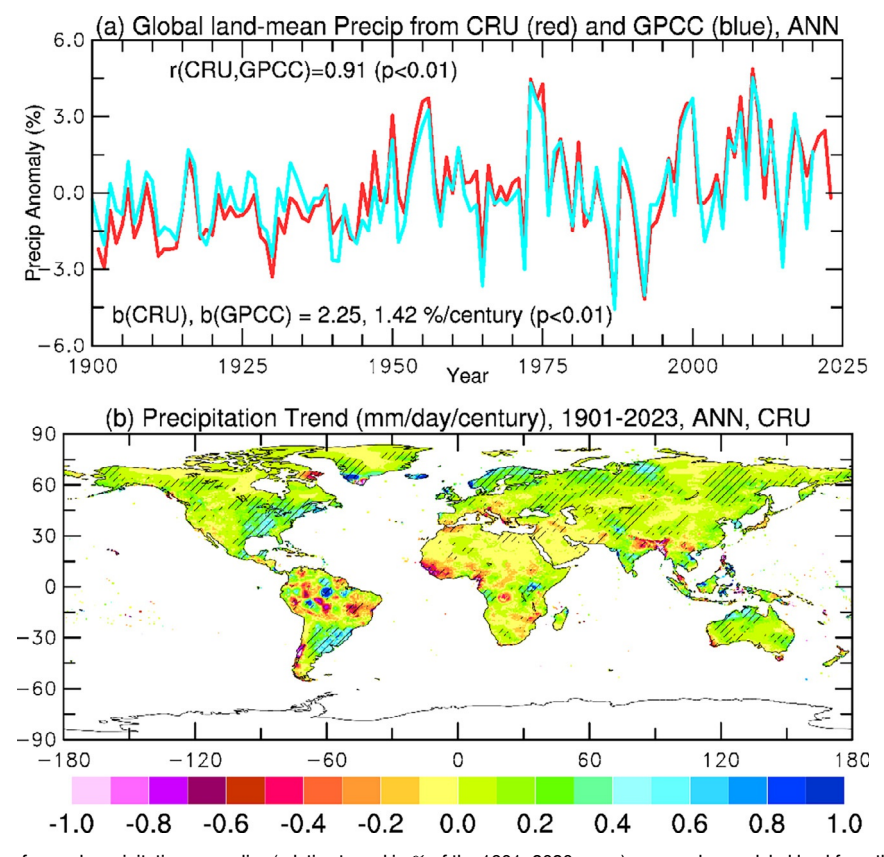


Fig. 12 (a) Time series of annual precipitation anomalies (relative to and in % of the 1901–2020 mean) averaged over global land from the CRU TS4.08 (red) and GPCC v2022 (blue) datasets derived from rain-gauge records. The correlation (t) between the two curves and their linear slopes (t) are shown on the panel together with their t-values. (b) Map of linear trends (in mm/day/century) during 1901–2023 based on the CRU dataset. Hatching indicates the trend is significant at the 5% level. Note that the precipitation data before 1950 are less reliable. Map lines delineate study areas and do not necessarily depict accepted national boundaries.

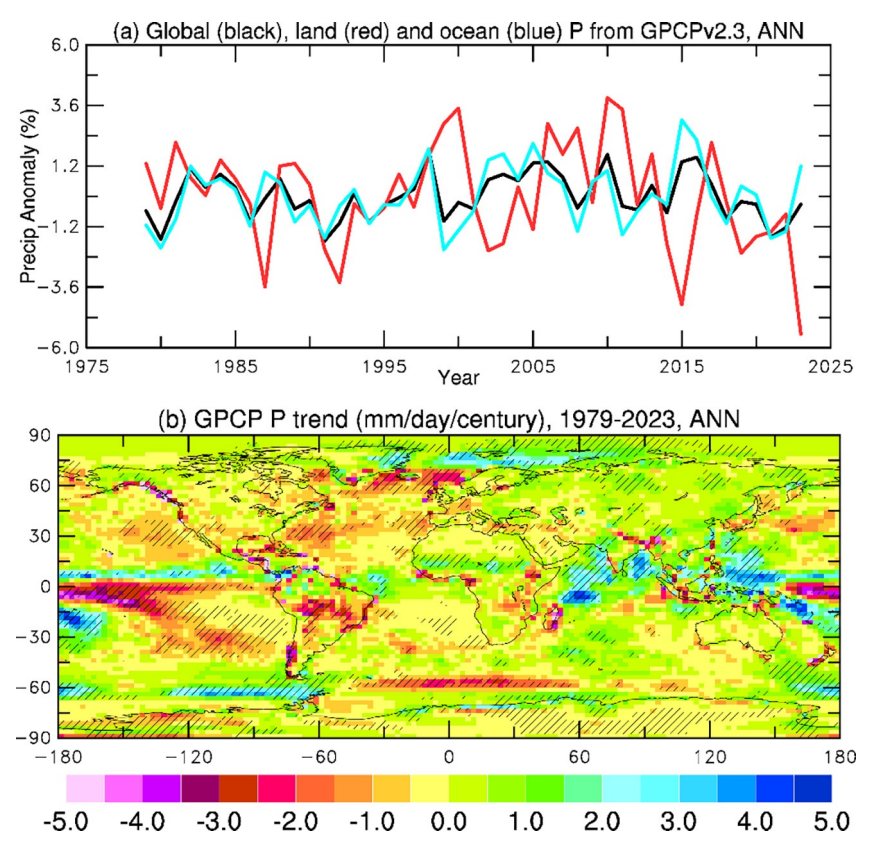


Fig. 13 (a) Time series of annual precipitation anomalies (in % of the 1979–2023 mean) averaged over the globe (black), global land (red) and ocean (blue) from 1979 to 2023 based on GPCP v2.3 dataset derived from rain-gauge (over land) and satellite (over ocean) observations. (b) Linear trend map of the GPCP annual precipitation during 1979–2023 in mm/day/century. Hatching indicates the trend is significant at the 5% level. Map lines delineate study areas and do not necessarily depict accepted national boundaries.

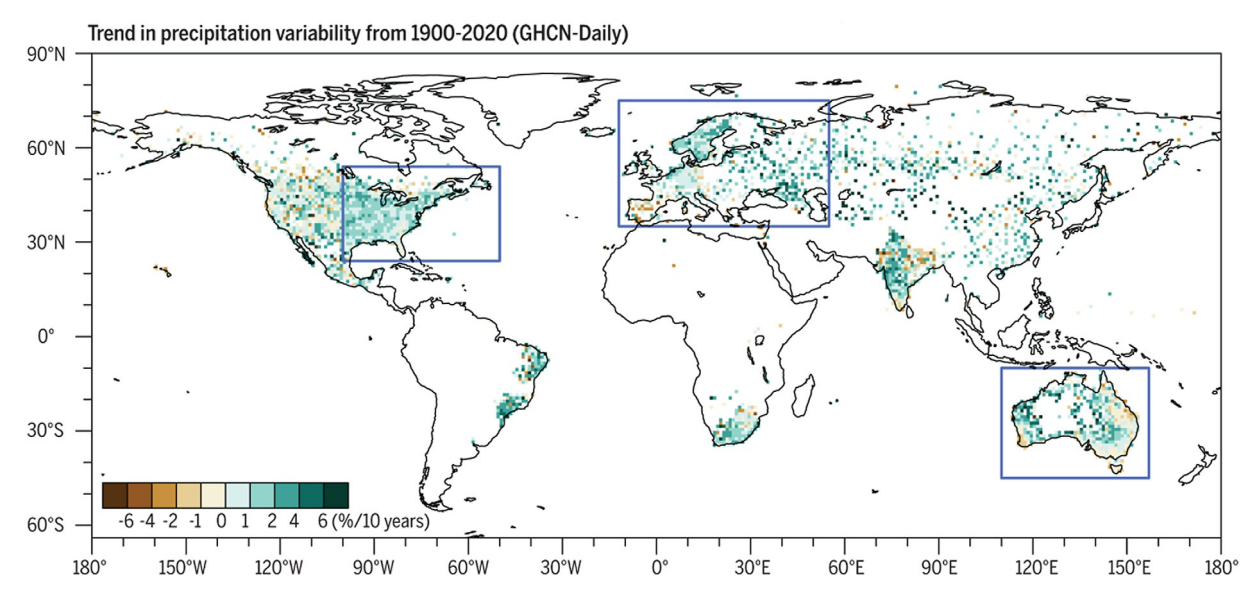


Fig. 14 Changes (in % change per decade) in the day-to-day variability of daily precipitation during 1900–2020 from station observations. Map lines delineate study areas and do not necessarily depict accepted national boundaries. Reproduced from Zhang W, Zhou T, and Wu P (2024) Anthropogenic amplification of precipitation variability over the past century. *Science* 385: 427–432. https://doi.org/10.1126/science.adp0212 with permission.

although historical increases in greenhouse gases appear to have generated an upward trend in global precipitation since 1979 (Gu and Adler, 2023). However, such a forced trend has not yet become statistically significant given the large natural fluctuations.

Besides the mean changes, day-to-day precipitation variability has increased over most land areas (Fig. 14) since 1900, which is driven primarily by increased greenhouse gases offset partially by increased aerosols (Zhang et al., 2024). Furthermore, precipitation frequency has decreased due to decreases in light-moderate precipitation events while precipitation intensity and heavy precipitation events have increased (Shiu et al., 2012; Ma et al., 2015). Such a change could lead to higher runoff and drier soils, and increased floods downstream (Dai et al., 2018; Wu et al., 2024).

Direct measurements of land evapotranspiration (ET) and oceanic evaporation (E) are unavailable over most regions; thus, they are often estimated using surface meteorological fields (from surface or satellite observations or reanalysis products) based on various equations such as the bulk formula for E. Because of inhomogeneity in surface wind and radiation records, long-term trends in surface E or ET from reanalysis products and other datasets often differ substantially and should be used with caution. Nevertheless, several diagnostic land ET products show an upward trend from 1982 to 2020, partly associated with increased precipitation and greening during the period over many land areas (Fig. 15; Yang et al., 2023). Oceanic E is often driven by decadal changes in surface wind speed, with a minimum in the 1970s and an upward trend thereafter with another wind-induced slowdown since 2008 (Fig. 16; Yu, 2007; Ma et al., 2025). Sea surface salinity (SSS) changes are a good measure of E-P; from 1960 to 2017 SSS records show increases over the tropical and subtropical Atlantic Ocean and western Indian Ocean, but decreases in the northern and western North Pacific, tropical Pacific, eastern Indian Ocean and Southern Ocean (Cheng et al., 2020).

Continental freshwater discharge can be estimated by summing up the river discharge (monitored continuously for most major rivers) around all coastal lines (Dai and Trenberth, 2002; Dai et al., 2009). Variations and changes in continental discharge are tightly coupled with land precipitation, which are influenced by tropical Pacific SSTs on interannual-decadal time scales (Fig. 17a). During 1950–2018, global continental discharge shows large year-to-year fluctuations, including the extremely low discharge in 1992 after the Pinatubo volcanic eruption, but with no clear trends (Fig. 17a). However, regionally, discharge in many rivers in Africa (including the Congo), South and East Asia, southern Europe, eastern Brazil and eastern Australia has decreased, while discharge from Russian rivers, the Mississippi, Amazon, and Parana has increased (Fig. 17b). Increased human withdrawals may have contributed to the declining streamflow over semiarid regions but likely had only small impacts over other regions (Dai et al., 2009). The discharge trend patterns are consistent with precipitation trends over land (Dai, 2021), which increases our confidence in these trends as precipitation and river discharge are measured independently.

Model-simulated response to global warming

Simulations of the water cycle in climate models

Climate models simulate many aspects of the global water cycle, including surface evaporation and transpiration, the water movement in the air and oceans, the water balance in the soil, atmosphere and ocean. However, many water cycle processes, such as the formation of clouds and precipitation, atmospheric convection, water movements on and under land surface, and transpiration by heterogeneous vegetation, happen on very small $(10^{-4}-10^3 \text{ m})$ scales that cannot be explicitly resolved by current climate models, which typically have a grid size of 50-150 km. These small-scale processes are often represented approximately

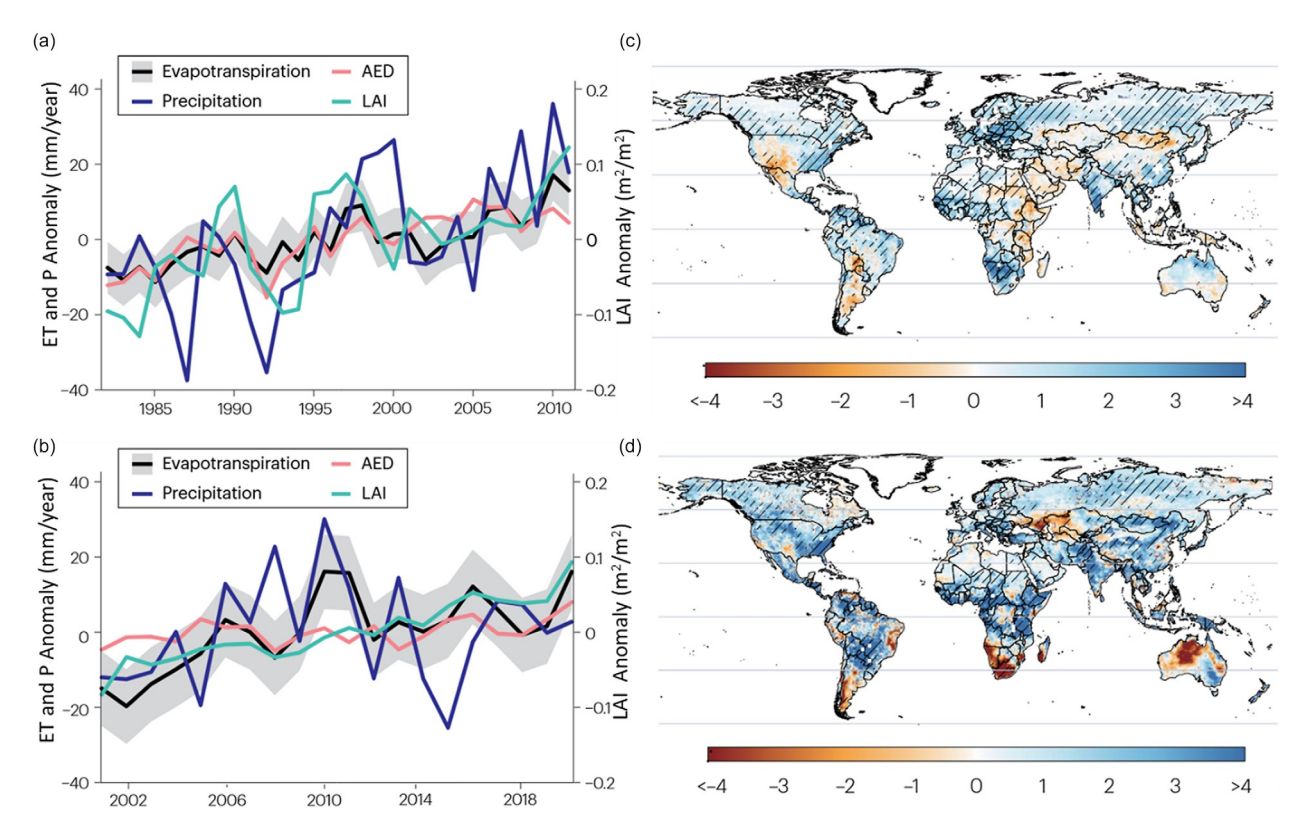


Fig. 15 (a-b) Time series of annual anomalies of global ET, precipitation, atmospheric evaporative demand (AED) and leaf area index (LAI) over land during (a) 1982–2011 and (b) 2001–2020; gray shading represents one standard deviation across multiple ET data sets. (c-d) Spatial pattern of the ET trends during (c) 1982–2011 and (d) 2001–2020; hatching represents areas with statistically significant trends (p < 0.05). The ET was estimated using seven (a, c) and five (b, d) diagnostic datasets. Map lines delineate study areas and do not necessarily depict accepted national boundaries. Reproduced from Yang Y et al. (2023) Evapotranspiration on a greening earth. *Nature Reviews Earth and Environment* 4: 626–641, https://doi.org/10.1038/s43017-023-00464-3 with permission.

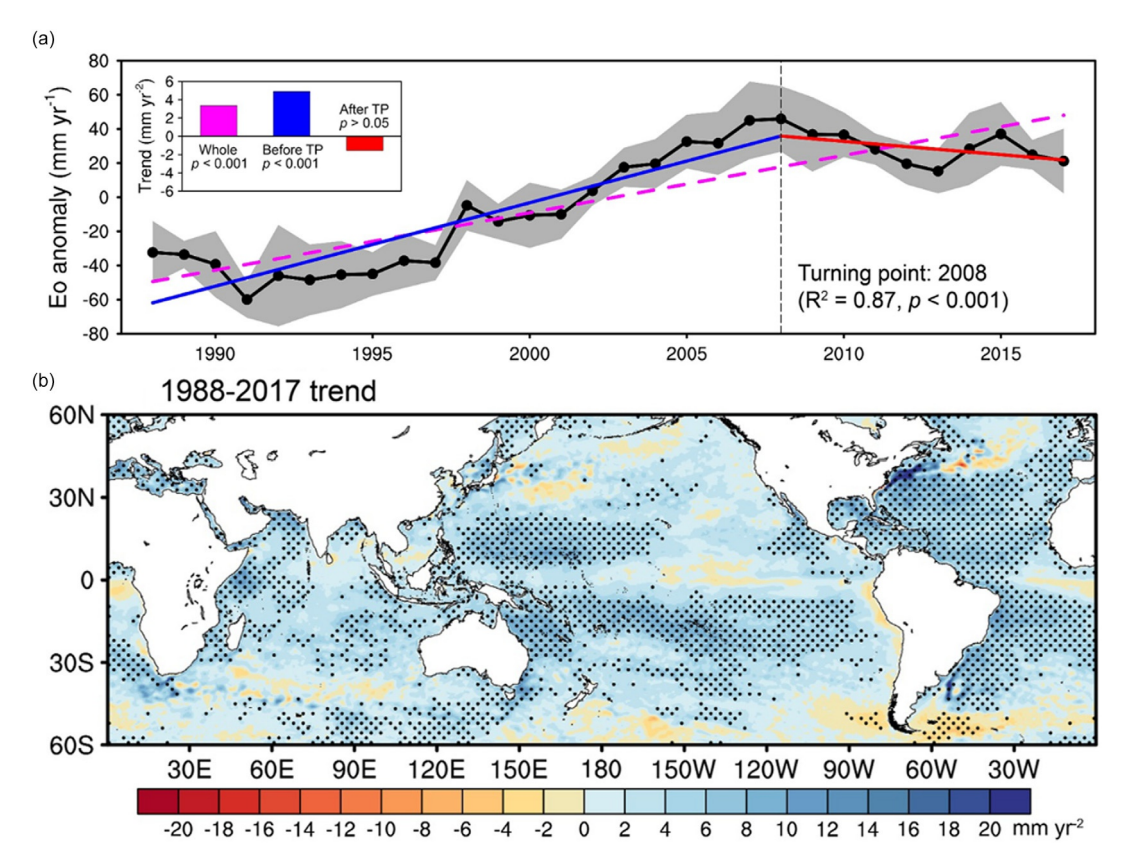


Fig. 16 (a) Anomaly time series in annual evaporation over global (60°S–60°N) oceans during 1988–2017. The black dot-line represents the ensemble mean of four satellite products, while the gray shading indicates ±1 standard deviation across these products. (b) Linear trend map of the annual evaporation during 1988–2017. Map lines delineate study areas and do not necessarily depict accepted national boundaries. Reproduced from Ma N, Zhang Y, and Yang Y (2025) Recent decline in global ocean evaporation due to wind stilling. *Geophysical Research Letters* 52: e2024GL114256. https://doi.org/10.1029/2024GL114256.

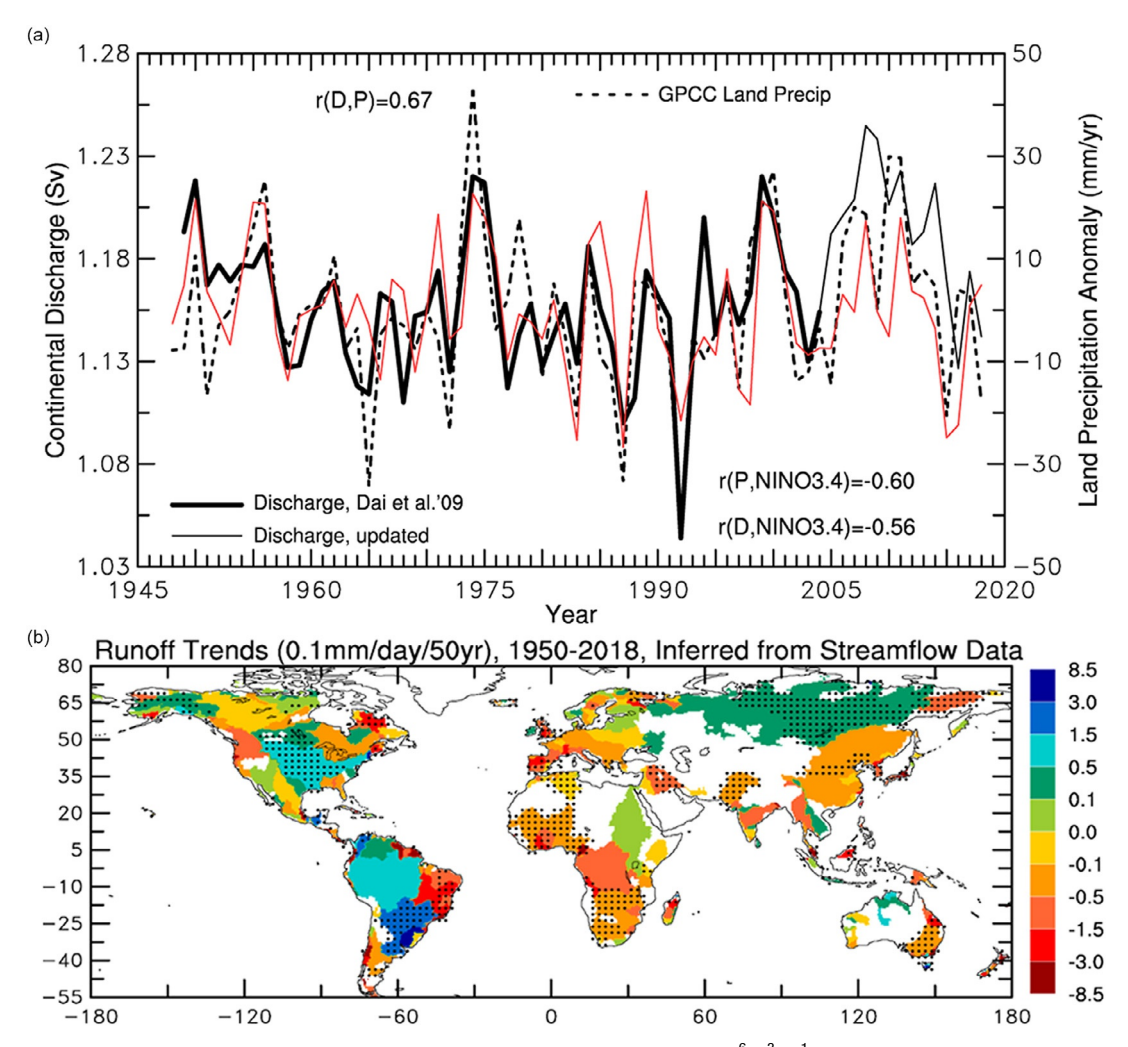


Fig. 17 (a) Yearly time series of October–September mean total continental discharge (in Sv or 1×10^6 m³ s $^{-1}$, excluding that from Greenland and Antarctica) for 1949–2018 (black solid line) estimated based on streamflow observations from 925 world's largest rivers. The dashed line is the October–September mean precipitation averaged over global (60° S– 75° N) land areas. The red line is the Niño3.4 (170° W– 120° W, 5° S– 5° N) SST index (positive downward, range from -3.0 to +3.0). Also shown are the correlation coefficients between the discharge (D), precipitation (P) and Nino3.4 index. The x-axis indicates the year of the September (e.g., 1948 refers to the average for 10/1947–9/1948). (b) Linear trends during 1950–2018 in annual runoff inferred from records of downstream river flow rates (in 0.1 mm/day per 50 years). Blank land areas do not have runoff into the oceans or do not have enough observations. Stippling indicates the trend is statistically significant at the 5% level. Map lines delineate study areas and do not necessarily depict accepted national boundaries. Reproduced from Dai A (2021) Hydroclimatic trends during 1950–2018 over global land. *Climate Dynamics* 56: 4027–4049. https://doi.org/10.1007/s00382-021-05684-1 with permission.

through parameterizations (i.e., using resolved large-scale fields to represent small-scale processes). Errors in simulating these processes lead to long-standing biases in model-simulated precipitation, clouds and other aspects of the water cycle.

For example, instead of an ITCZ from about 5 to 15°N and a South Pacific Convergence Zone (SPCZ) lying southeast of New Guinea (see Fig. 2a), coupled global climate models still produce a secondary rainband south of the equator in the central-eastern Pacific – the so-called double ITCZ problem that is likely linked to deficiencies in the simulated air-sea interactions in the region (Tian and Dong, 2020). Climate models also rain too frequently at reduced intensity – the chronic "drizzle problem" that is partly due to coarse model resolution and too much convective precipitation produced by their cumulus convection schemes (Dai, 2006; Trenberth et al., 2017; Chen et al., 2021). The drizzle bias is also reflected by the underestimated high-frequency fluctuations of precipitation in models (Covey et al., 2018). Model-simulated warm-season precipitation tends to peak soon after noon over land, in contrast to late afternoon in observations (Lee and Wang, 2021; Tang et al., 2021). As a result, global climate models tend to underestimate heavy precipitation but overestimate light-moderate precipitation, although convection-permitting simulations with km grid sizes improve the precipitation histograms and diurnal cycle greatly (Dai et al., 2020; Rasmussen et al., 2023).

Other major deficiencies in model-simulated water cycles include (1) unrealistic formation of clouds and their response to global warming (Zelinka et al., 2022); (2) insufficient vertical exchange of water between the root zone and the deeper layer that can lead to large warm and dry biases in the interior of the continents during the warm season (Barlage et al., 2021), and 3) lack of dynamic glaciers and polar icesheets.

Model-simulated response of the water cycle

Many studies have examined model-simulated response of precipitation, water vapor, clouds, soil moisture, runoff, and other aspects of the water cycle to increasing GHGs in the 21st century under various emissions scenarios, which include projections of future emissions of GHGs and aerosols as well as land use changes. Despite known shortcomings, climate models simulate the large-scale climate *response* to projected future GHG changes, representing a long-term systematic change from current conditions. It will be superimposed on top of the unpredictable future natural fluctuations in weather and climate. To estimate the response to future GHG changes, the internal variability that can lead to different trends in regional precipitation over periods of multiple decades needs to be removed, often through averaging over many ensemble simulations whose internal variations are uncorrelated.

Climate models project large increases in annual precipitation over the northern mid-high latitudes and the equatorial Pacific in the 21st century under moderate-to-high emissions scenario, but decreases over many subtropical land and oceanic areas such as Central America, northern South America, the Mediterranean region, the subtropical southeastern Pacific, subtropical Atlantic, and subtropical Indian Ocean (Fig. 18a; Collins et al., 2013; Lee et al., 2021). Precipitation change patterns are very similar under different emissions scenarios (Huang et al., 2020; Zhao and Dai, 2022). The increases in northern mid-high latitude precipitation can be explained by large increases in water vapor and the large increase in equatorial precipitation is due to increased moisture convergence in tropical convection in a warmer climate (Chou et al., 2009), while the decreases in subtropical precipitation result from the enhanced drying effect of the subsidence as the vertical gradient of specific humidity and Hadley overturning circulation increase (Zhu et al., 2023).

As expected, precipitation frequency decreases both in recent observations (Shiu et al., 2012; Ma et al., 2015) and model projections (Dai et al., 2018) due to decreases in light-moderate precipitation events, while precipitation intensity and heavy precipitation events increase. Physically, the decrease in light-moderate precipitation events is caused by increased low-level negative buoyancy due to a slight decrease in near-surface RH over land (Chen et al., 2020), likely linked to drier soils (Zhao and Dai, 2022). The lower near-surface RH suppresses weak convection that produces light-moderate rain events but allows positive buoyancy to accumulate in the atmosphere that eventually produces intense but fewer storms. From a water vapor supply (by evaporation) and depletion (by precipitation) perspective, the larger increase in rainstorm intensity (\geq 7 %/K) than in evaporation (\sim 2%/K for global-mean) also implies that in the future it may take longer for evaporation to replenish the water vapor depleted by the previous rainstorm before the next one can form, leading to a slightly longer dry interval between rainstorms in the future, which is confirmed in 4 km downscaling simulations (Dai et al., 2020).

While changes in precipitation, especially its amount (A), have attracted the most attention, changes in surface evaporation (or ET over land), runoff and soil moisture are also of great concern. With increased heating from elevated GHGs, evaporation is

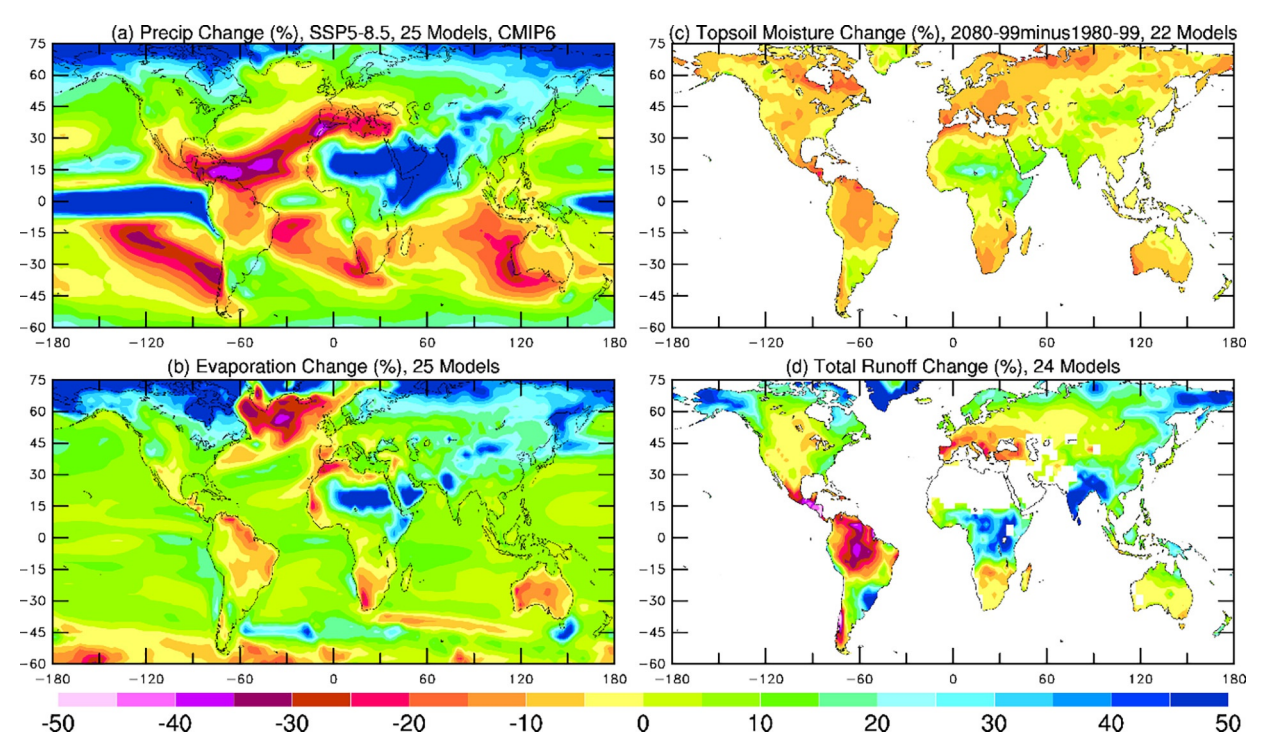


Fig. 18 Projected percentage changes from 1980 to 1999 to 2080–2099 in annual (a) precipitation, (b) surface evaporation (including transpiration over land), (c) top 10 cm soil moisture, and (d) total runoff averaged over 25 runs from 25 CMIP6 models for (a-b), 22 runs from 22 models for (c) and 24 runs form 24 models for (d) under the SSP5–8.5 emissions scenario. Areas with little mean runoff are masked out in (d). Map lines delineate study areas and do not necessarily depict accepted national boundaries.

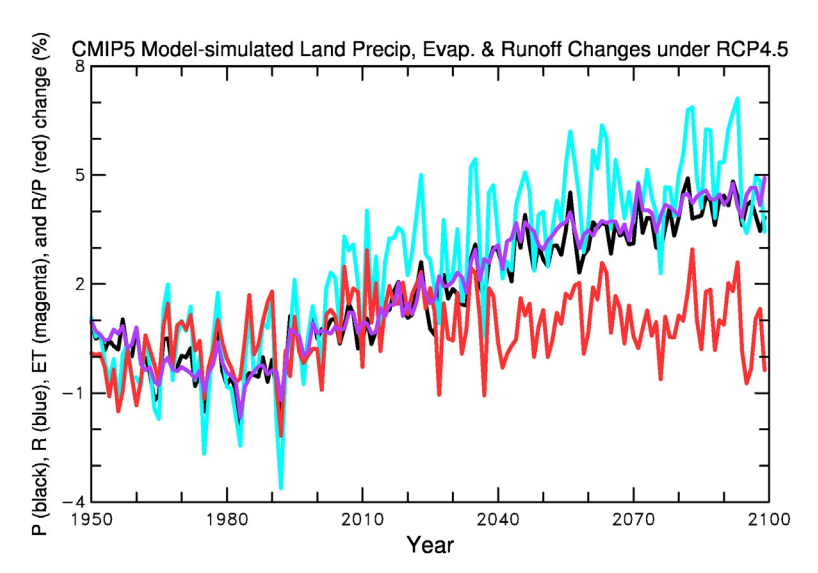


Fig. 19 Time series of the changes (relative to and in percentage of the 1950–1979 mean) in globally (60°S–75°N) averaged land annual precipitation (P, black line), total runoff (R, blue), evapotranspiration (ET, magenta), and runoff ratio (R/P) (red) derived from 14 (12 for R) CMIP5 models under the low-moderate RCP4.5 scenario. The 1950–1979 mean for the global land P, R, ET, and R/P are 2.340, 0.709, 1.690 mm/day, and 0.303, respectively. Reproduced from Zhao T and Dai A (2015) The magnitude and causes of global drought changes in the 21st century under a low-moderate emissions scenario. *Journal of Climate* 28: 4490–4512. https://doi.org/10.1175/JCLI-D-14-00363.1 with permission. © American Meteorological Society.

projected to increase over wet surfaces, such as the oceans except for the northern North Atlantic (Fig. 18b) (Dai, 2022). Local oceanic evaporation changes depend on several factors such as SST and wind changes and mean wind strength (Chen et al., 2019). Land ET change patterns depend on water availability and thus largely follow changes of precipitation amounts. However, land ET is often limited by the availability of soil water, especially in the subtropics and arid regions. Indeed, climate models project widespread decreases in topsoil moisture in the 21st century, even over areas with increasing precipitation (Fig. 18c). This leads to increased risk of droughts and wildfires. The drying of the topsoil results from decreased precipitation in the subtropics and ubiquitous increases in evaporative demand under rising air temperatures and slight decreases in land surface RH (Lee et al., 2021), both leading to increases in surface vapor pressure deficit which drives up evaporative demand (Scheff and Frierson, 2014; Zhao and Dai, 2022). A less examined contributor is the decreased precipitation frequency and increased intensity, which should lengthen the dry spells and possibly increase runoff, leading to drier soils (Dai et al., 2018). Decreases in subsurface soil moisture are not as widespread as the topsoil moisture and resembles changes in total runoff (Berg et al., 2017; Zhao and Dai, 2022).

Total runoff changes largely follow precipitation change patterns, with increases in the northern high latitudes and most of Asia and central Africa, but decreases over northern South America, Central America, and southern Europe (Fig. 18d; Zhao and Dai, 2022). This is expected as precipitation is the primary driver of runoff.

As precipitation amount over global land increases, land-averaged ET increases steadily, following land precipitation in percentage changes (Fig. 19). Continental runoff, which reflects the net amount of water vapor transported from the ocean to land, also increases together with land precipitation amount, with similar percentage increases but large variations in global runoff ratio (Fig. 19). While the global runoff ratio is slightly higher in the 21st century than during 1950–1999, it does not show an upward trend as one might expect, given the increasing precipitation intensity and heavy precipitation. One possible offsetting factor is the land surface drying with decreasing soil moisture (Fig. 18c; Zhao and Dai, 2015, 2022), which should increase infiltration and reduce runoff during a rainstorm.

These model results are just a small sample of those available, as many different emissions scenarios have been explored by researchers. Changes in extremes such as tropical cyclones are important but not discussed here.

Summary and challenges

Water is essential for all lives on Earth. It acts as an agent of erosion, plays a key role in human civilizations and in Earth's weather and climate. In particular, water vapor in the atmosphere keeps Earth's surface temperatures above the freezing point over most places and provides the water source for clouds and precipitation. Its strong dependence on air temperature roughly doubles the warming directly caused by an increase in CO₂ and other greenhouse gases, but its short lifetime means that water vapor provides strong positive feedback rather than a forcing for climate change.

Water moves around the Earth system, via atmospheric winds and ocean currents, and on land in rivers and streams. Heating on Earth's surface leads to **evaporation** from water or wet land surfaces or **transpiration** from plants. Once in the air, water vapor can travel thousands of kilometers away from the source during its average lifetime of about 10 days before returning to the surface

through **precipitation**. Precipitation requires 1) cooling of an air parcel to saturation, often by upward motion, 2) condensation of water vapor to form clouds, 3) growth and fallout of cloud droplets, and 4) continued supply of water vapor by winds. Rainfall causes **infiltration** into land. When the soil becomes saturated or the rain rate exceeds the infiltration rate, a lateral water flow occurs, generating **runoff**, which converges into streams and rivers and eventually discharges into oceans in a few weeks. Over global land, runoff generates about 38,000 km³/yr freshwater discharge into the oceans, which is about 10 times the freshwater used by human society. However, this renewable freshwater resource is unevenly distributed, so that people living in arid and semi-arid regions are under water stress.

Under global warming, the global water cycle is expected to accelerate as the global-mean evaporation and precipitation are expected to increase by $\sim 2\%$ /°C, which is determined by changes in surface and atmospheric energy balance. Whereas precipitation intensity is expected to increase by $\geq 7\%$ /°C because of increased water vapor (by $\sim 7\%$ /°C) and thus moisture convergence during a rainstorm, precipitation frequency is expected to decrease mainly due to fewer light-moderate precipitation events while heavy precipitation becomes more frequent. Over land, the decrease in light-moderate precipitation events is caused by a slight decrease in near-surface RH linked to drier soils. The faster increase in rainstorm intensity than in surface evaporation suggests that it may take longer for evaporation to replenish the water vapor depleted by the previous storm before the next one can occur, leading to longer dry spells and thus fewer but stronger precipitation events in a future warmer climate.

While annual precipitation amount is projected to increase in the deep tropics (due to increased moisture convergence in deep convection) and over mid-high latitudes (due to increased water vapor), it would decrease in the subtropics with downward motion, which may strengthen and dry the mid-lower troposphere more effectively due to increased vertical gradients of water vapor. Evaporation is projected to increase over most oceans and most land areas with increasing precipitation, where runoff also increases. On land, rising air temperatures and slight decreases in surface RH lead to ubiquitous increases in atmospheric demand for moisture, leading to widespread drying in topsoil moisture, especially over subtropical regions with decreasing precipitation. This increases the risk of drought and wildfire.

There are many challenges in studying the global water cycle and its long-term changes. A lack of reliable, long-term observations for evaporation, runoff, soil moisture and oceanic precipitation hinders accurate water balance analysis and long-term change studies. The basic processes underlying the global water cycle are understood reasonably well; however, it has been a major challenge to represent these processes in numerical models due to their complexity and small scales $(10^{-4}-10^3 \text{ m})$. Climate models still tend to rain too frequently at reduced intensity, partly due to their coarse resolution. They also have difficulties in simulating the formation of clouds and precipitation, atmospheric convective systems, and the heterogeneity of land surface, again partly due to their coarse resolution. Improved understanding and simulation of polar ice sheets are also needed. As climate models are increasingly run at kilometer resolution, many of these biases should diminish in the next 10-20 years.

Acknowledgments

Dai is supported by the National Science Foundation (Grant #AGS-2015780 & 2528650). The National Center for Atmospheric Research is sponsored by the National Science Foundation.

References

Barlage M, Chen F, Rasmussen R, Zhang Z, and Miguez-Macho G (2021) The importance of scale-dependent groundwater processes in land-atmosphere interactions over the central United States. *Geophysical Research Letters* 48: e2020GL092171. https://doi.org/10.1029/2020GL092171.

Beck HE, Pan M, Miralles DG, Reichle RH, Dorigo WA, Hahn S, et al. (2021) Evaluation of 18 satellite-and model-based soil moisture products using in situ measurements from 826 sensors. *Hydrology and Earth System Sciences* 25: 17–40. https://doi.org/10.5194/hess-25-17-2021.

Berg A, Sheffield J, and Milly PCD (2017) Divergent surface and total soil moisture projections under global warming. *Geophysical Research Letters* 44: 236–244. https://doi.org/10.1002/2016GL071921.

Chen J, Dai A, and Zhang Y (2019) Projected changes in daily variability and seasonal cycle of near-surface air temperature over the globe during the 21st century. *Journal of Climate* 32: 8537–8561. https://doi.org/10.1175/JCLI-D-19-0438.1.

Chen J, Dai A, and Zhang Y (2020) Linkage between projected precipitation and atmospheric thermodynamic changes. *Journal of Climate* 33: 7155–7178. https://doi.org/10.1175/ JCLI-D-19-0785.1.

Chen D, Dai A, and Hall A (2021) The convective-to-total precipitation ratio and the "drizzling" bias in climate models. *Journal of Geophysical Research* 126: e2020JD034198. https://doi.org/10.1029/2020JD034198.

Cheng S, Guan X, Huang J, Ji F, and Guo R (2015) Long-term trend and variability of soil moisture over East Asia. *Journal of Geophysical Research – Atmospheres* 120: 8658–8670. https://doi.org/10.1002/2015JD023206.

Cheng L, Trenberth KE, Gruber N, et al. (2020) Improved estimates of changes in upper ocean salinity and the hydrological cycle. *Journal of Climate* 33: 10357–10381. https://doi.org/10.1175/JCLI-D-20-0366.1.

Chou C, Neelin JD, Chen C-A, and Tu J-Y (2009) Evaluating the "rich-get-richer" mechanism in tropical precipitation change under global warming. *Journal of Climate* 22: 1982–2005.

Collins M, et al. (2013) Long-term climate change: Projections, commitments and irreversibility. In: Stocker TF, et al. (eds.) Climate Change 2013: The Physical Science Basis.

Contribution of Working Group I to the Fifth Assessment Report of the Intergovernmental Panel on Climate Change, pp. 1029–1136. Cambridge, United Kingdom and New York, NY, USA: Cambridge University Press. https://doi.org/10.1017/cbo9781107415324.024.

Covey C, Doutriaux C, Gleckler PJ, Taylor KE, Trenberth KE, and Zhang Y (2018) High-frequency intermittency in observed and model-simulated precipitation. *Geophysical Research Letters* 45: 12,514–12,522. https://doi.org/10.1029/2018GL078926.

Dai A (2006) Precipitation characteristics in eighteen coupled climate models. Journal of Climate 19: 4605–4630.

Dai A (2008) Temperature and pressure dependence of the rain-snow phase transition over land and ocean. *Geophysical Research Letters* 35: L12802. https://doi.org/10.1029/2008GL033295.

Dai A (2021) Hydroclimatic trends during 1950-2018 over global land. Climate Dynamics 56: 4027-4049. https://doi.org/10.1007/s00382-021-05684-1.

Dai A (2022) Arctic amplification is the main cause of the Atlantic meridional overturning circulation weakening under large CO₂ increases. *Climate Dynamics* 58: 3243–3259. https://doi.org/10.1007/s00382-021-06096-x.

Dai A (2024) The diurnal cycle from observations and ERA5 in precipitation, clouds, boundary layer height, buoyancy, and surface fluxes. Climate Dynamics 62: 5879–5908. https://doi.org/10.1007/s00382-024-07182-6.

Dai A and Bloecker CE (2019) Impacts of internal variability on temperature and precipitation trends in large ensemble simulations by two climate models. Climate Dynamics 52: 289–306. https://doi.org/10.1007/s00382-018-4132-4.

Dai A and Trenberth KE (2002) Estimates of freshwater discharge from continents: Latitudinal and seasonal variations. Journal of Hydrometeorology 3: 660-687.

Dai A, Del Genio AD, and Fung IY (1997) Clouds, precipitation, and temperature range. Nature 386: 665-666.

Dai A, Trenberth KE, and Karl TR (1999) Effects of clouds, soil moisture, precipitation and water vapor on diurnal temperature range. Journal of Climate 12: 2451–2473.

Dai A, Qian T, Trenberth KE, and Milliman JD (2009) Changes in continental freshwater discharge from 1949-2004. Journal of Climate 22: 2773–2791

Dai A, Wang J, Thorne PW, Parker DE, Haimberger L, and Wang XL (2011) A new approach to homogenize daily radiosonde humidity data. Journal of Climate 24: 965–991.

Dai A, Zhao T, and Chen J (2018) Climate change and drought: A precipitation and evaporation perspective. *Current Climate Change Reports* 4: 301–312. https://doi.org/10.1007/s40641-018-0101-6. http://link.springer.com/article/10.1007/s40641-018-0101-6.

Dai A, Rasmussen RM, Liu C, Ikeda K, and Prein AF (2020) A new mechanism for warm-season precipitation response to global warming based on convection-permitting simulations. Climate Dynamics 55: 343–368. https://doi.org/10.1007/s00382-017-3787-6.

Deser C, Knutti R, Solomon S, and Phillips AS (2012) Communication of the role of natural variability in future North American climate. *Nature Climate Change* 2: 775–779. https://doi.org/10.1038/nclimate1562.

Dingman SL (2015) Physical Hydrology, 3rd edn. Waveland Press. 643 pp.

Dong B and Dai A (2015) The influence of the Inter-decadal Pacific Oscillation on temperature and precipitation over the globe. Climate Dynamics 45: 2667–2681. https://doi.org/10.1007/s00382-015-2500-x.

Miller JB (2024) Global climate [in "state of the climate in 2023"]. In: Dunn RJH, Blannin J, Gobron N, and Willett KM (eds.) Bulletin of the American Meteorological Society (BAMS), vol. 105, pp. S12–S155. https://doi.org/10.1175/BAMS-D-24-0116.1.

Fasullo J (2011) A mechanism for land—ocean contrasts in global monsoon trends in a warming climate. Climate Dynamics 39: 1137–1147. https://doi.org/10.1007/s00382-011-

Gu G and Adler R (2023) Observed variability and trends in global precipitation during 1979–2020. Climate Dynamics 61: 131–150. https://doi.org/10.1007/s00382-022-06567-9. Gulev SK, et al. (2021) Changing state of the climate system. In: Masson-Delmotte V, et al. (eds.) Climate Change 2021: The Physical Science Basis. Contribution of Working Group I to the Sixth Assessment Report of the Intergovernmental Panel on Climate Change, pp. 287–422. Cambridge, United Kingdom and New York, NY, USA: Cambridge University Press. https://doi.org/10.1017/9781009157896.004.

Hartmann DL, et al. (2013) Observations: Atmosphere and surface. In: Stocker TF, et al. (eds.) Climate Change 2013: The Physical Science Basis. Contribution of Working Group I to the Fifth Assessment Report of the Intergovernmental Panel on Climate Change. Cambridge, United Kingdom and New York, NY, USA: Cambridge University Press.

Hegerl GC, et al. (2015) Challenges in quantifying changes in the global water cycle. Bulletin of the American Meteorological Society (BAMS) 96: 1097—1115. https://doi.org/10.1175/BAMS-D-13-00212.1.

Huang D, Dai A, and Zhu J (2020) Are the transient and equilibrium climate change patterns similar in response to increased CO₂? *Journal of Climate* 33: 8003–8023. https://doi.org/10.1175/JCLI-D-19-0749.1.

Hugonnet R, et al. (2021) Accelerated global glacier mass loss in the early twenty-first century. Nature 592: 726-731.

Ingleby B, Moore D, Sloan C, and Dunn R (2013) Evolution and accuracy of surface humidity reports. *Journal of Atmospheric and Oceanic Technology* 30: 2025–2043. https://doi.org/10.1175/JTFCH-D-12-00232.1.

Jasechko S, Seybold H, Perrone D, Fan Y, Shamsudduha M, Taylor RG, Fallatah O, and Kirchner JW (2024) Rapid groundwater decline and some cases of recovery in aquifers globally. Nature 625: 715–721.

Kuang, et al. (2024) The changing nature of groundwater in the global water cycle. Science 383: eadf0630. https://doi.org/10.1126/science.adf0630.

Lee Y-C and Wang Y-C (2021) Evaluating diurnal rainfall signal performance from CMIP5 to CMIP6. Journal of Climate 34: 7607–7623. https://doi.org/10.1175/JCLI-D-20-0812.1.

Lee J-Y, et al. (2021) Future global climate: Scenario-based projections and near-term information. In: Masson-Delmotte V, et al. (eds.) Climate Change 2021: The Physical Science Basis. Contribution of Working Group I to the Sixth Assessment Report of the Intergovernmental Panel on Climate Change, pp. 553—672. Cambridge, United Kingdom and New York, NY, USA: Cambridge University Press. https://doi.org/10.1017/9781009157896.006.

Li Z, Yan ZW, Zhu YN, Freychet N, and Tett S (2020) Homogenized daily relative humidity series in China during 1960–2017. Advances in Atmospheric Sciences 37: 318–327. https://doi.org/10.1007/s00376-020-9180-0.

Ma S, Zhou T, Dai A, and Han Z (2015) Observed changes in the distributions of daily precipitation frequency and amount over China from 1960–2013. *Journal of Climate* 28: 6960–6978. https://doi.org/10.1175/JCLI-D-15-0011.1.

Ma N, Zhang Y, and Yang Y (2025) Recent decline in global ocean evaporation due to wind stilling. *Geophysical Research Letters* 52: e2024GL114256. https://doi.org/10.1029/2024GL114256.

Mouginot J, et al. (2019) Forty-six years of Greenland Ice Sheet mass balance from 1972 to 2018. *Proceedings. National Academy of Sciences. United States of America* 116: 9239–9244.

Muñoz-Sabater J, Dutra E, Agustí-Panareda A, Albergel C, Arduini G, Balsamo G, et al. (2021) ERA5-Land: A state-of-the-art global reanalysis dataset for land applications. *Earth System Science Data* 13: 4349–4383. https://doi.org/10.5194/essd-13-4349-2021.

Norris JR and Evan AT (2015) Empirical removal of artifacts from the ISCCP and PATMOS-x satellite cloud records. *Journal of Atmospheric and Oceanic Technology* 32: 691–702. https://doi.org/10.1175/JTECH-D-14-00058.1.

Norris JR, Allen RJ, Evan AT, Zelinka MD, O'Dell CW, and Klein SA (2016) Evidence for climate change in the satellite cloud record. *Nature* 536: 72–75. https://doi.org/10.1038/nature18273.

Qin M, Dai A, and Zhang R (2022) A review of Atlantic multidecadal variability. Advances in Earth Science (in Chinese) 27: 963–978. https://doi.org/10.11867/j.issn.1001-8166.2022.059.

Rasmussen RM, Chen F, Liu C, Ikeda K, Prein A, Kim J, Schneider T, Dai A, et al. (2023) CONUS404: The NCAR-USGS 4-km long-term regional hydroclimate reanalysis over the CONUS. Bulletin of the American Meteorological Society (BAMS) 104: E1382–E1408. https://doi.org/10.1175/BAMS-D-21-0326.1.

Scanlon BR, et al. (2023) Global water resources and the role of groundwater in a resilient water future. Nature Reviews Earth and Environment 4: 87–101.

Scheff J and Frierson DMW (2014) Scaling potential evapotranspiration with greenhouse warming. *Journal of Climate* 27: 1539–1558. https://doi.org/10.1175/JCLI-D-13-00233.1. Schmidt GA, Ruedy RA, Miller RL, and Lacis AA (2010) Attribution of the present-day total greenhouse effect. *Journal of Geophysical Research* 115: D20106. https://doi.org/10.1029/2010JD014287.

Shiu CJ, Liu SC, Fu C, Dai A, and Sun Y (2012) How much do precipitation extremes change in a warming climate? *Geophysical Research Letters* 39: L17707. https://doi.org/10.1029/2012GL052762.

Smith B, Fricker HA, Gardner AS, et al. (2020) Pervasive ice sheet mass loss reflects competing ocean and atmosphere processes. *Science* 368: 1239–1242. https://doi.org/10.1126/science.aaz5845.

Stubenrauch CJ, et al. (2024) Lessons learned from the updated GEWEX cloud assessment database. Surveys in Geophysics 45: 1999–2048. https://doi.org/10.1007/s10712-024-09824-0

Swain DL, Prein AF, Abatzoglou JT, et al. (2025) Hydroclimate volatility on a warming Earth. *Nature Reviews Earth and Environment* 6: 35–50. https://doi.org/10.1038/s43017-024-00624-z.

Tang S, Gleckler P, Xie S, Lee J, Ahn M-S, Covey C, and Zhang C (2021) Evaluating diurnal and semi-diurnal cycle of precipitation in CMIP6 models using satellite- and ground-based observations. *Journal of Climate* 34: 3189–3210.

Tian B and Dong X (2020) The double-ITCZ Bias in CMIP3, CMIP5 and CMIP6 models based on annual mean precipitation. *Geophysical Research Letters* 47: e2020GL087232. https://doi.org/10.1029/2020GL087232.

Trenberth KE (2011) Changes in precipitation with climate change. Climate Research 47: 123-138. https://doi.org/10.3354/cr00953.

Trenberth KE (2022) The Changing Flow of Energy through the Climate System. Cambridge University Press, 319 pp. https://doi.org/10.1017/9781108979030.

Trenberth KE and Cheng L (2024) Earth's energy balance. In: Reference Module in Earth Systems and Environmental Sciences. Elsevier. https://doi.org/10.1016/B978-0-323-96026-7.00039-4. (ISBN 9780124095489).

Trenberth KE and Zhang Y (2018) How often does it really rain? *Bulletin of the American Meteorological Society (BAMS*) 99: 289–298. https://doi.org/10.1175/BAMS-D-17-0107.1.

Trenberth KE, Smith L, Qian T, Dai A, and Fasullo J (2007a) Estimates of the global water budget and its annual cycle using observational and model data. *Journal of Hydrometeorology* 8: 758–769.

Trenberth KE, et al. (2007b) Observations: Surface and atmospheric climate change. In: Solomon S, et al. (eds.) Climate Change 2007: The Physical Science Basis. Contribution of Working Group I to the Fourth Assessment Report of the Intergovernmental Panel on Climate Change. Cambridge, United Kingdom and New York, NY, USA: Cambridge University Press

Trenberth KE, Dai A, Rasmussen RM, and Parsons DB (2003) The changing character of precipitation. Bulletin of the American Meteorological Society 84: 1205-1217.

Trenberth KE, Fasullo JT, and Mackaro J (2011) Atmospheric moisture transports from ocean to land and global energy flows in reanalyses. *Journal of Climate* 24: 4907–4924. https://doi.org/10.1175/2011JCLI4171.1.

Trenberth KE, Zhang Y, and Gehne M (2017) Intermittency in precipitation: duration, frequency, intensity, and amounts using hourly data. *Journal of Hydrometeorology* 18: 1393–1412. https://doi.org/10.1175/JHM-D-16-0263.1.

Trenberth KE, Cheng L, Jacobs P, Zhang Y, and Fasullo J (2018) Hurricane Harvey links to ocean heat content. *Earth's Future* 6: 730–744. https://doi.org/10.1029/2018EF000825. Trenberth KE, Cheng L, Pan Y, Fasullo J, and Mayer M (2025) Distinctive pattern of global warming in ocean heat content. *Journal of Climate* 38: 2155–2168. https://doi.org/10.1175/JCLI-D-24-0609.1

Tselioudis G, Rossow WB, Bender F, Oreopoulos L, and Remillard J (2024) Oceanic cloud trends during the satellite era and their radiative signatures. Climate Dynamics 62: 9319–9332. https://doi.org/10.1007/s00382-024-07396-8.

Wan N, Lin X, Pielke RA Sr, Zeng X, and Nelson AM (2024) Global total precipitable water variations and trends over the period 1958–2021. *Hydrology and Earth System Sciences* 28: 2123–2137. https://doi.org/10.5194/hess-28-2123-2024.

Wang K and Dickinson RE (2012) A review of global terrestrial evapotranspiration: Observation, modeling, climatology, and climatic variability. *Reviews of Geophysics* 50: RG2005. https://doi.org/10.1029/2011RG000373.

Wang JA, Dai CM, and Zhang L (2016) Global water vapor trend from 1988-2011 and its diurnal asymmetry based on GPS, radiosonde, and microwave satellite measurements. Journal of Climate 29: 5205–5222. https://doi.org/10.1175/JCLI-D-15-0485.1.

Warren SG, Eastman RM, and Hahn CJ (2007) A survey of changes in cloud cover and cloud types over land from surface observations, 1971–96. *Journal of Climate* 20: 717–738. WGMS (2023) Global glacier change bulletin no. 5 (2020–2021). In: Zemp M, Gärtner-Roer I, Nussbaumer SU, Welty EZ, Dussaillant I, and Bannwart J (eds.) *ISC(WDS)/IUGG(IACS)/UNEP/UNESCO/WMO, World Glacier Monitoring Service, Zurich, Switzerland*, 134 pp., publication based on database version:. https://doi.org/10.5904/wgms-fog-2023-09.

Wu Y, Yin X, Zhou G, Bruijnzeel LA, Dai A, Wang F, Gentine P, Zhang G, Song Y, and Zhou D (2024) Rising rainfall intensity induces spatially divergent hydrological changes within a large river basin. *Nature Communications* 15: 823. https://doi.org/10.1038/s41467-023-44562-8.

Yang Y, et al. (2023) Evapotranspiration on a greening earth. Nature Reviews Earth and Environment 4: 626-641. https://doi.org/10.1038/s43017-023-00464-3.

Yu L (2007) Global variations in oceanic evaporation (1958–2005): The role of the changing wind speed. *Journal of Climate* 20: 5376–5390. https://doi.org/10.1175/2007.JCI.11714.1.

Zelinka MD, Klein SA, Qin Y, and Myers TA (2022) Evaluating climate models' cloud feedbacks against expert judgment. Journal of Geophysical Research – Atmospheres 127: e2021JD035198. https://doi.org/10.1029/2021JD035198.

Zhang W, Zhou T, and Wu P (2024) Anthropogenic amplification of precipitation variability over the past century. *Science* 385: 427–432. https://doi.org/10.1126/science.adp0212. Zhao T and Dai A (2015) The magnitude and causes of global drought changes in the 21st century under a low-moderate emissions scenario. *Journal of Climate* 28: 4490–4512. https://doi.org/10.1175/JCLI-D-14-00363.1.

Zhao T and Dai A (2022) CMIP6 model-projected hydroclimatic and drought changes and their causes in the 21st century. *Journal of Climate* 35: 897–921. https://doi.org/10.1175/ JCII-D-21-0442.1.

Zhong Z, He B, Chen HW, et al. (2023) Reversed asymmetric warming of sub-diurnal temperature over land during recent decades. *Nature Communications* 14: 7189. https://doi.org/10.1038/s41467-023-43007-6.

Zhu P, Jia X, Zhao C, and Shao M (2022) Long-term soil moisture evolution and its driving factors across China's agroecosystems. *Agricultural Water Management* 269: 107735. https://doi.org/10.1016/j.agwat.2022.107735.

Zhu J, Dai A, Huang D, Xiao X, and Liu Y (2023) Subtropical drying under greenhouse gas-induced warming. Climate Dynamics 61: 4219–4242. https://doi.org/10.1007/s00382-023-06797-5.